

Growth Factor Independence 1 Antagonizes a p53-Induced DNA Damage Response Pathway in Lymphoblastic Leukemia

Cyrus Khandanpour,^{1,3,9} James D. Phelan,^{4,9,10} Lothar Vassen,¹ Judith Schütte,⁶ Riyan Chen,¹ Shane R. Horman,^{4,11} Marie-Claude Gaudreau,^{1,2} Joseph Krongold,^{1,7} Jinfang Zhu,⁸ William E. Paul,⁸ Ulrich Dührsen,³ Bertie Göttgens,⁶ H. Leighton Grimes,^{4,5,*} and Tarik Möröy^{1,2,7,*}

¹Institut de recherches cliniques de Montréal (IRCM), 110 Avenue des Pins Ouest, Montréal, Québec H2W 1R7, Canada

²Département de Microbiologie et Immunologie, Université de Montréal, Montréal, Québec H3C 3J7, Canada

³Department of Haematology, University Hospital, University Duisburg-Essen, Hufelandstrasse 55, 45122 Essen, Germany

⁴Division of Cellular and Molecular Immunology

⁵Division of Experimental Hematology

Cincinnati Children's Hospital Medical Center, Cincinnati, OH 45229, USA

⁶Cambridge Institute for Medical Research and Wellcome Trust-Medical Research Council Cambridge Stem Cell Institute, University of Cambridge, Cambridge CB2 0XY, UK

⁷Division of Experimental Medicine, McGill University, Montreal, Québec H3A 1A3, Canada

⁸Laboratory of Immunology, National Institute of Allergy and Infectious Disease, National Institutes of Health, Bethesda, MD 20829, USA

⁹These authors contributed equally to this work

¹⁰Present address: Metabolism Branch, Center for Cancer Research, National Cancer Institute, National Institutes of Health, Bethesda, MD 20892, USA

¹¹Present address: Genomics Institute of the Novartis Research Foundation, San Diego, CA 92121, USA

*Correspondence: lee.grimes@cchmc.org (H.L.G.), tarik.moroy@ircm.qc.ca (T.M.)

<http://dx.doi.org/10.1016/j.ccr.2013.01.011>

SUMMARY

Most patients with acute lymphoblastic leukemia (ALL) fail current treatments highlighting the need for better therapies. Because oncogenic signaling activates a p53-dependent DNA damage response and apoptosis, leukemic cells must devise appropriate countermeasures. We show here that growth factor independence 1 (Gfi1) can serve such a function because Gfi1 ablation exacerbates p53 responses and lowers the threshold for p53-induced cell death. Specifically, Gfi1 restricts p53 activity and expression of proapoptotic p53 targets such as *Bax*, *Noxa* (*Pmaip1*), and *Puma* (*Bbc3*). Subsequently, Gfi1 ablation cures mice from leukemia and limits the expansion of primary human T-ALL xenografts in mice. This suggests that targeting Gfi1 could improve the prognosis of patients with T-ALL or other lymphoid leukemias.

INTRODUCTION

Many patients with acute lymphoblastic leukemia (ALL) and lymphoma die of tumor relapse (Gökbuget and Hoelzer, 2009). Experiments with mouse models have shown that T-ALL-like diseases can be accelerated by the overexpression of the transcriptional repressor growth factor independence 1 (Gfi1), which

is a well-established nuclear zinc finger protein and regulator of lymphoid development (Gilks et al., 1993; Zörnig et al., 1996; Li et al., 2010; Pargmann et al., 2007; Spooner et al., 2009; Yücel et al., 2003). Germline *Gfi1* deletion in mice modestly reduces thymic cellularity, with an accumulation of cells between double-negative 1 (DN1) and DN2 stages as well as a skew from CD4⁺ to CD8⁺ (Yücel et al., 2003). In contrast, the thymus is

Significance

Chemotherapy is nonspecific and highly toxic, damaging both host and tumor tissues. Even when effective, patients suffer dramatic side effects from standard treatments. Molecular-based targeted therapies have shown great promise but lack broad applicability due to the heterogeneity of oncogenic pathways mutated during transformation. Here, we demonstrate that ablation of Gfi1 broadly leads to lymphoid tumor regression and host survival independent of the transforming pathway. We demonstrate that Gfi1 limits the proapoptotic functions of the endogenous gatekeeper p53. Gfi1 inhibition amplifies p53-dependent proapoptotic responses driven by oncogenic stress; consequently, transformed lymphoid tissues are uniquely susceptible to Gfi1 inhibition. Thus, in combination with current therapies, Gfi1 inhibition may allow the use of lower cytotoxic doses, which would benefit patients directly.

relatively normal when *Gfi1* is deleted after the DN stage (Zhu et al., 2006), which suggests that Gfi1 mainly acts during early steps of T lymphopoiesis. Gfi1's ability to accelerate leukemogenesis in mice and its function in lymphoid development prompted us to explore the role of Gfi1 ablation in the initiation or maintenance of lymphoid malignancies.

RESULTS

***GFI1* Is Associated with a Subgroup of Human T-ALL and Accelerates NOTCH1-Induced T-ALL in Mice**

Although the oncogenic impact of high-level Gfi1 expression in murine T cell leukemogenesis is well established, an association of *GFI1* with human T-ALL has not been clearly shown. Because over 50% of human T-ALL displays mutated *NOTCH1* (Weng et al., 2004) or Notch1 regulatory proteins (O'Neil et al., 2007; Thompson et al., 2007) resulting in overexpression of Notch1 target genes (Palomero et al., 2006; Sharma et al., 2006; Weng et al., 2006), we performed hierarchical clustering of microarray data from independent cohorts of patients with T-ALL using *NOTCH1* mutation status (Ferrando et al., 2002), Notch1 target gene activation (Palomero et al., 2006; Van Vlierberghe et al., 2008), or early T cell precursor (ETP)-ALL diagnosis (Coustans-Smith et al., 2009) and examined *GFI1* expression (Figures 1A and 1B; Figures S1A–S1F available online).

We observed that patients with ETP-ALL had low levels of *GFI1* expression compared to those with a positive *NOTCH1* signature (Figures 1B, S1D, and S1E), suggesting a functional role for Gfi1 in *NOTCH1*-dependent human T-ALL. However, *GFI1* is unlikely a Notch1 target because intracellular Notch1 (ICN) does not occupy the *GFI1* locus nor was *GFI1* expression altered by γ -secretase inhibitors (GSIs) based on our own results as well as published data (Figure S1F) (Margolin et al., 2009; Medyouf et al., 2011). Also, we can show that mice transplanted with bone marrow (BM) cells overexpressing ICN and Gfi1 developed leukemia faster than mice transplanted with cells only overexpressing ICN (Figures S1G–S1I), corroborating previous reports on the function of Gfi1 in T cell leukemogenesis (Schmidt et al., 1998; Zörnig et al., 1996) and extending it to human ICN-mediated T-ALL.

***Gfi1* Deletion Delays the Development of T-ALL**

To test whether ablation of Gfi1 could inhibit the onset of T-ALL, we used five different mouse models, in which we could temporally delete *Gfi1*. First, we transplanted ICN-expressing BM cells from mice carrying a tamoxifen (OHT)-inducible *Rosa26* Cre-recombinase transgene (*Cre^{ERT2}*) (Hameyer et al., 2007) enabling inducible deletion of floxed *Gfi1* alleles (*Gfi1^{fl/fl}*) (Horman et al., 2009; Velu et al., 2009) (Figure 1C). Although vehicle-treated animals died within 66 days, OHT-treated recipients developed leukemia within 87 days with similar T-ALL characteristics (Figures 1C–1F). However, all tumors emerging after OHT treatment had intact *Gfi1* alleles (Figure 1D), suggesting that ICN-induced T-ALL selects for Gfi1.

To confirm this, we used a T cell-specific Cre transgene (*LckCre⁺*) and *Gfi1^{fl/Δ}* transgenic mice, in which *Rosa26* locus-mediated expression of ICN and EGFP is blocked by a floxed STOP cassette (*Rosa^{ICN^{LSL}}*) (Murtaugh et al., 2003). We injected these mice with N-ethyl-N-nitrosourea (ENU), which

induces T cell leukemia and shortens the latency of leukemogenesis (Kundu et al., 2005; Yuan et al., 2001). Approximately 50% of all tumors arising in *LckCre⁺;Rosa^{ICN^{LSL}};Gfi1^{+/+}* mice were EGFP⁺ (i.e., expressing ICN and Gfi1, Figures S1J and S1K). However, ENU-induced tumors that arose in *LckCre⁺;Rosa^{ICN^{LSL}};Gfi1^{fl/Δ}* mice were always EGFP⁻ (i.e., ICN⁻ and Gfi1 wild-type, Figure S1K), also suggesting that ICN-mediated tumorigenesis selects for Gfi1. In yet another Notch-driven leukemogenesis model, in which constitutive absence of *Gfi1* was coupled with a *CD4* promoter-driven mutant Notch1 transgene (*Notch1^{ΔCT}*; Priceputu et al., 2006), T-ALL development was substantially decreased and delayed (Figures 1G–1I).

To explore the impact of *Gfi1* loss in mouse models of T-ALL that are not initiated by Notch, we either infected *Gfi1^{+/+}* and *Gfi1^{-/-}* newborn mice with Murine Moloney Leukemia (MMLV) (Scheijen et al., 1997) or injected adolescent mice with ENU. All MMLV-infected *Gfi1^{+/+}* mice developed lymphoid malignancies, whereas only 40% of MMLV-infected *Gfi1^{-/-}* mice did. The remaining mice were censored due to neurological problems consistent with reports on older *Gfi1^{-/-}* mice (unpublished data). Notably, *Gfi1^{-/-}* lymphoid malignancies were significantly less robust than *Gfi1^{+/+}* tumors (Figures 1J–1L). Similarly, >85% of the ENU-injected *Gfi1^{+/+}* mice, but only 20% of *Gfi1^{-/-}* mice, developed T cell leukemia (Figure S1L); the remaining mice succumbed to ENU-induced toxicity. As in other models, ENU-initiated *Gfi1^{-/-}* tumors developed slower and were significantly less robust than *Gfi1^{+/+}* tumors (Figures S1L–S1N). Neither *Gfi1^{+/+}* nor *Gfi1^{-/-}* ENU-induced tumors were found to harbor *Notch1* mutations in the HD or PEST domain (Table S1). Thus, results from these five independent T-ALL models, initiated by various oncogenic pathways, led us to conclude that ablation of *Gfi1* delays, impedes, or is counterselected during T-ALL formation.

T-ALL Disease Maintenance Is Gfi1 Dependent

Mx1-Cre⁺;Gfi1^{fl/fl} or *Gfi1^{fl/fl}* mice were treated with ENU to elicit T cell leukemia. After 50 days, both groups were injected with plpC (Horman et al., 2009). All *Gfi1^{fl/fl}* mice developed T-ALL, but *Mx1-Cre⁺;Gfi1^{fl/fl}* mice separated into two different subgroups following plpC injection. One subgroup remained healthy until the study was terminated (Figure 2A, *Mx1-Cre⁺;Gfi1^{fl/fl}*, full excision) or died of ENU toxicity. The second subgroup displayed partial *Gfi1* deletion and succumbed to T cell leukemia similar to ENU/plpC-treated *Gfi1^{fl/fl}* mice (Figure 2A, *Mx1-Cre⁺;Gfi1^{fl/fl}* partial excision).

To investigate whether loss of *Gfi1* was causing tumor regression or preventing tumor formation, we used ultrasound imaging. Upon detection of a tumor (Figure 2B), *Gfi1* deletion was induced with plpC. All ENU-induced tumors in *Gfi1^{fl/fl}* mice clearly showed increases in tumor size, whereas tumors that developed in *Mx1-Cre⁺;Gfi1^{fl/fl}* animals showed variable changes in size (Figures 2C and S2A). Following plpC injection, disease-free survival, tumor growth, and blast cell detection all directly correlated with the degree of *Gfi1* deletion in the tumor (Figures 2B, 2C, and S2B) because we found that *Gfi1* deletion was incomplete in tumors that progressed but was complete in tumors that regressed (Figure S2A).

We verified this observation in a second T-ALL model, in which disease was induced by Notch1 activation and

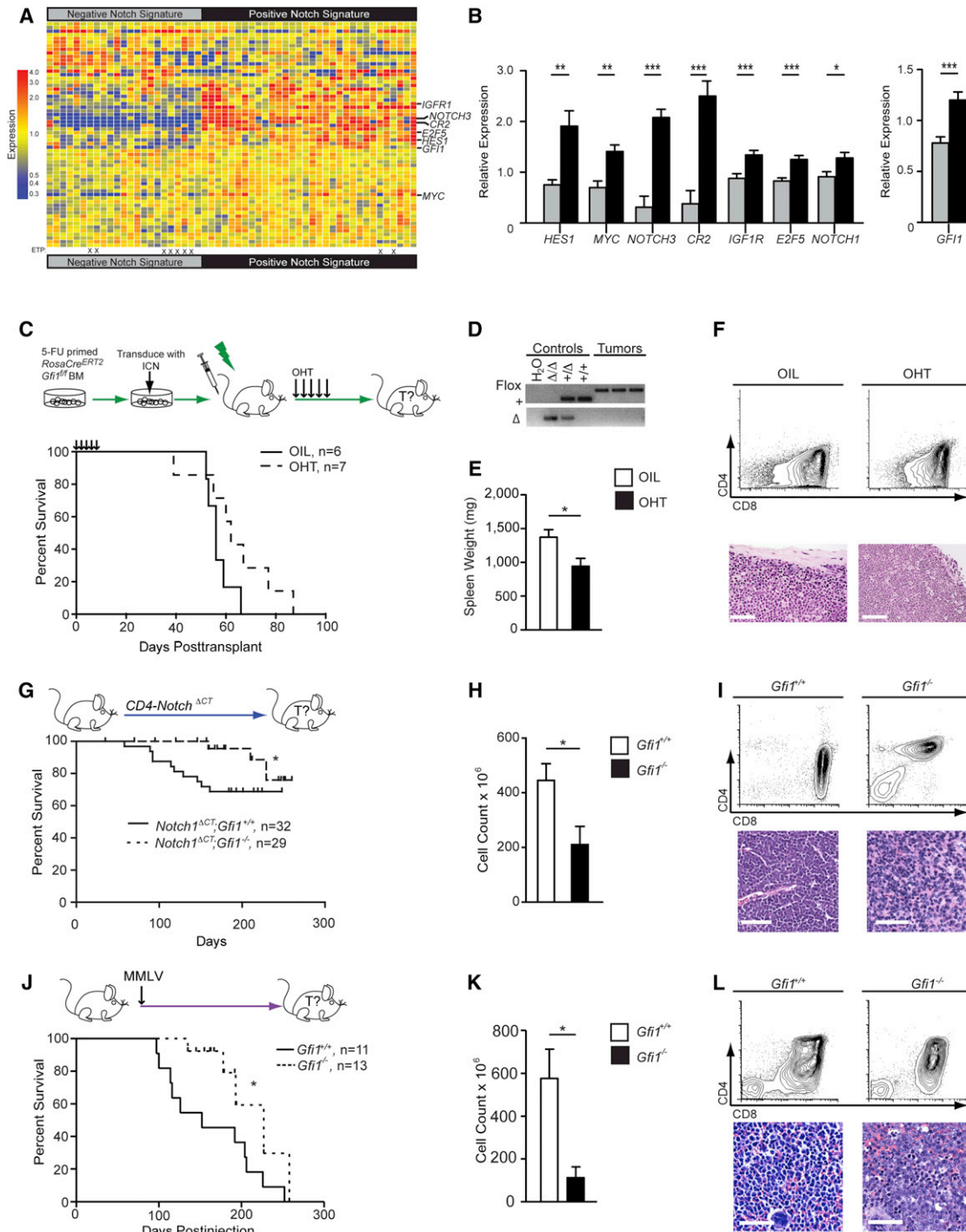


Figure 1. Gfi1 Associates with NOTCH1 in Human T-ALL, and Deletion Delays the Development of Disease
 (A) Heatmap of expression of published Notch1 target genes used to classify gene expression array data from 55 patients with T-ALL (GSE8879) into two groups: "Negative Notch Signature" (left), and "Positive Notch Signature" (right). ETP-ALL diagnosis is designated by an "X."
 (B) Quantification of relative expression of *NOTCH1*, *Gfi1*, and Notch1 target genes *HES1*, *MYC*, *NOTCH3*, *CR2*, *IGF1R*, and *E2F5* in 55 patients with T-ALL with either a "Negative Notch Signature" (gray) or a "Positive Notch Signature" (black).
 (C) Top view shows *RosaCre^{ERT2};Gfi1^{fl/fl}* BM cells that were transduced with vectors expressing ICN and then transplanted. Mice were given vehicle or tamoxifen to induce Cre activity. Bottom view is a Kaplan-Meier curve.
 (D) PCR genotype analysis of the *Gfi1* locus in control tissues (*Gfi1*^{Δ/Δ}, *Gfi1*^{+/-Δ}, *Gfi1*^{+/-+}) and in representative tumors from mice either treated with vehicle or OHT. FLOX, *Gfi1*^{fl} allele; +, the wild-type allele; Δ, deleted allele.
 (E and F) Spleen weights (E; n = 6 each group) and flow cytometric analysis of thymic tumors (F, top panels) and spleen sections with H&E (F, bottom panels) collected during postmortems from indicated transplant groups.

(legend continued on next page)

accelerated by ENU injection. Mice were monitored by ultrasound and upon tumor detection, treated with plpC (Figure 2D). Although all plpC-injected *Notch1^{ΔCT};Gfi1^{fl/fl}* mice died, all plpC-injected *Notch1^{ΔCT};Mx1-Cre⁺;Gfi1^{fl/fl}* tumors with complete deletion of *Gfi1* regressed, and the mice survived (Figures 2D–2F). This regression also correlated with lower numbers of blast cells in the blood of plpC-treated *Notch1^{ΔCT};Mx1-Cre⁺;Gfi1^{fl/fl}* mice compared to *Notch1^{ΔCT};Gfi1^{fl/fl}* controls (Figure S2C).

Next, *Gfi1^{fl/fl}* or *Mx1-Cre⁺;Gfi1^{fl/Δ}* tumor cells were transplanted into syngeneic recipients. In recipients that did not receive plpC, only tumors with an intact floxed *Gfi1* allele emerged (data not shown). However, when recipient mice were treated with plpC, all mice that received *Gfi1^{fl/fl}* tumors died, whereas mice receiving *Mx1-Cre⁺;Gfi1^{fl/Δ}* tumors survived tumor free (Figure 2G). To demonstrate that loss of *Gfi1* specifically leads to tumor regression in a cell-autonomous manner, we inhibited *Gfi1* function in three Tal1-transformed murine T-ALL cell lines (Cullion et al., 2009) by overexpressing a dsRed-marked *Gfi1* dominant-negative mutant (*Gfi1^{N382S}*) (Horman et al., 2009; Person et al., 2003; Zarebski et al., 2008). Two days after the initial measurement of transduction, and in contrast to empty vector-transduced cells, only 15%–20% of cells transduced with dsRed⁺ *Gfi1^{N382S}*-expressing vectors were still dsRed⁺ (Figure 2H).

To determine the clinical potential of targeting *Gfi1*, we injected *Gfi1^{fl/fl}* and *Mx1-Cre⁺;Gfi1^{fl/fl}* mice (CD45.2⁺) with ENU, waited 50 days to allow tumor initiation, and then treated with plpC to delete *Gfi1*. Four weeks after the first plpC injection, both groups of mice were sublethally irradiated and transplanted with syngeneic CD45.1⁺ BM cells (BMT) to prevent BM failure associated with ENU (Figures 2I and 2J). The combination therapy was not sufficient to cure the mice of T-ALL because 80% of ENU-treated *Gfi1^{fl/fl}* mice still succumbed to disease (one died of nontumor-related reasons). However, when therapy was combined with *Gfi1* deletion, complete tumor remission was observed in every transplant recipient (Figures 2I and 2J). Taken together, our data strongly implicate *Gfi1* in the maintenance of established T cell malignancies, their ability to kill secondary hosts, and potentially in improving therapy.

Maintenance of B Cell Lymphoma Is Dependent on *Gfi1*

To test whether other lymphoid malignancies were also dependent on *Gfi1*, we used *Eμ-Myc* transgenic mice, which develop clonal B cell lymphomas (Adams et al., 1985). Loss of *Gfi1* did not affect the latency, incidence, or pathology of tumor initiation (Figures 3A and 3B) but completely blocked the ability of

lymphoma to kill secondary recipients (Figure S3A). Thus, similar to the T cell models, *Gfi1* is required for robust tumorigenesis. To determine whether *Gfi1* is required for B cell lymphoma maintenance, we used an inducible model (Zhu et al., 2006) to delete *Gfi1^{fl/fl}* after a lymphoma had formed. Although plpC injection had no effect on progression of disease in *Gfi1^{fl/fl};Eμ-Myc* mice, it led to tumor regression and a significant reduction of leukemic blasts in the peripheral blood of *Mx1-Cre⁺;Gfi1^{fl/fl};Eμ-Myc* mice (Figures 3C–3E and S3B), suggesting that *Gfi1* is indeed necessary to maintain a B cell lymphoma. Similar to the results with our T-ALL models, loss of *Gfi1* significantly improved the outcome of *Gfi1^{-/-};Eμ-Myc* mice treated with sublethal irradiation and BMT after detection of a tumor, whereas *Gfi1^{+/+};Eμ-Myc* animals died of tumor relapse (Figure 3F). These data suggest that targeting *Gfi1* could also be beneficial for treating B cell lymphoma.

Gfi1 Integrates the Cellular Transcriptional Response to DNA Damage/p53 Induction

To investigate how loss of *Gfi1* induces tumor regression, we compared gene expression profiles of T cell leukemia from two different models (Figures 2A and 2D) upon inducible deletion of *Gfi1* (Figure 4A). Gene Set Enrichment Analysis (GSEA) (Subramanian et al., 2005) demonstrated significant deregulation of multiple key leukemic pathways, including cell-cycle progression, NFκB signaling, and basal transcription among others (Table S2; data not shown). Normal thymocytes do not disappear upon loss of *Gfi1* as the tumors do. Therefore, to identify mechanisms that might explain tumor regression, we focused on those pathways that were similarly deregulated in both ENU and *Notch1^{ΔCT}*-induced tumors from *Gfi1^{-/-}* and *Gfi1^{+/+}* mice but were not enriched in normal nonmalignant *Gfi1^{-/-}* versus *Gfi1^{+/+}* thymocytes. We noticed a striking number of shared GSEA signatures that included deregulated p53 signaling, DNA damage/repair pathways, and a proapoptotic response (Figures 4B and 4C; Table S2), suggesting that an accelerated cell death program might be initiated in tumor cells that lack *Gfi1*.

An emerging concept proposes that oncogenic signaling induces uncoordinated cell division, generating collapsed replication forks and DNA double-strand breaks, which in turn initiate a DNA damage response, activating p53 and inducing apoptosis. Therefore, tumor cells must counteract cell death in order to survive (Bartek et al., 2007; Bartkova et al., 2007; Di Micco et al., 2006; Halazonetis et al., 2008). In agreement with this theory, leukemic cells from our tumor models displayed increased levels of phosphorylated H2AX (γH2AX), indicating DNA double-strand breaks, and higher levels of spontaneous

(G) Top view shows *Notch1^{ΔCT};Gfi1^{+/+}* and *Notch1^{ΔCT};Gfi1^{-/-}* mice that were monitored for tumor development and survival. Bottom view is a Kaplan-Meier curve.

(H and I) Spleen weights (H) and flow cytometric analysis (I, top panels) and histological sections (I, bottom panels) of *Notch1^{ΔCT};Gfi1^{+/+}* (n = 7) and *Notch1^{ΔCT};Gfi1^{-/-}* (n = 3) tumors.

(J) Top view shows *Gfi1^{+/+}* and *Gfi1^{-/-}* newborn mice that were injected with MMLV. Bottom view is a Kaplan-Meier curve.

(K) Thymic tumor cell numbers of *Notch1^{ΔCT}*-induced tumors.

(L) Flow cytometric analysis (top panels) and histological section (bottom panels) of MMLV-induced *Gfi1^{+/+}* versus *Gfi1^{-/-}* tumors.

Scale bars, 50 μm. Vertical line (|) in all Kaplan-Meier curves indicates censored mice. Mean and mean ± SEM are shown unless stated otherwise. *p < 0.05, **p < 0.01, ***p < 0.001.

See also Figure S1 and Table S1.

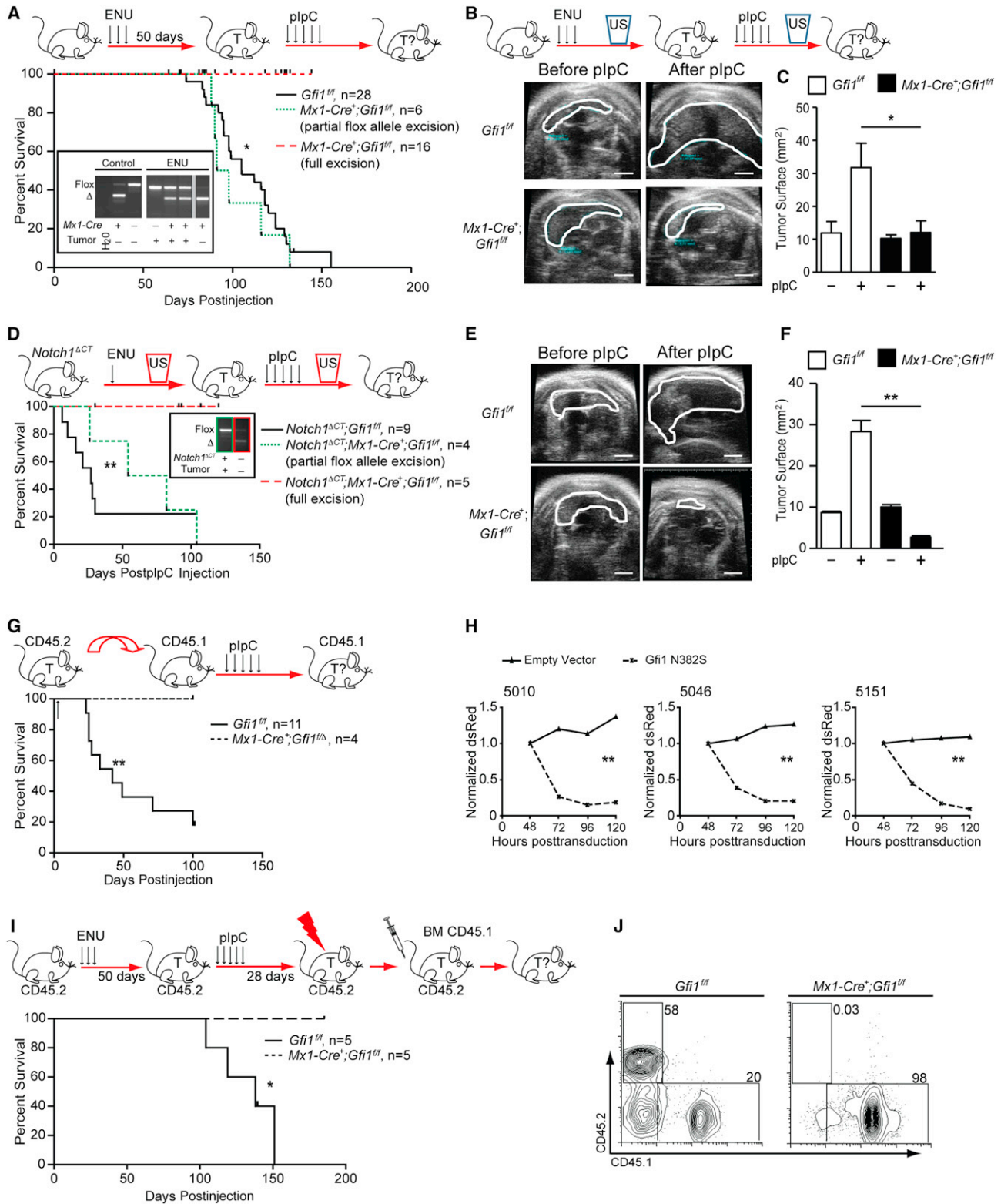


Figure 2. Gfi1 Is Required for T Cell Leukemia Maintenance

(A) Top view shows *Gfi1^{f/f}* or *Mx1-Cre⁺;Gfi1^{f/f}* mice that were treated with ENU and subsequently with plpC. Bottom view is a Kaplan-Meier curve. Inset presents PCR analysis of the *Gfi1* locus in control tissues and in representative tumors (T) for *Gfi1* flox and excised (Δ) alleles. (B) Top view shows *Gfi1^{f/f}* or *Mx1-Cre⁺;Gfi1^{f/f}* mice that were treated with ENU and followed for tumors by ultrasound (US). Next, mice were treated with plpC, and tumor development was determined by ultrasound. Bottom view is representative ultrasound images. Scale bars, 20 mm.

(legend continued on next page)

apoptosis than untransformed thymocytes (Figures 4D–4F). We also noted that the number of apoptotic cells was further increased in those tumors where *Gfi1* was inducibly deleted (Figure 4F). Additionally, when we irradiated *Gfi1*^{-/-} leukemic cells, we observed decreased survival compared to *Gfi1*^{+/+} tumors (Figures 4G). Finally, when we overexpressed *Bcl2* in Tal1-transformed T cell lines, counterselection of the dominant-negative mutant *Gfi1*^{N382S} was either absent or delayed (compare Figure 4H to Figure 2H). These data demonstrate that *Gfi1* is required in lymphoid tumors to counter DNA damage-induced death and suggest that DNA damage/p53-induced signals are dominant effectors of *Gfi1* loss-of-function apoptotic phenotypes in T-ALL.

In contrast to *Gfi1*-deleted tumors, *Gfi1*^{-/-} thymocytes display only mildly increased levels of apoptosis of c-Kit⁺ subsets (compared to *Gfi1*^{+/+}) (Yücel et al., 2003). In agreement with this observation, we noted that whereas GSEA of gene expression data of *Gfi1*^{-/-} versus *Gfi1*^{+/+} thymocytes is enriched for apoptotic signatures, the DNA damage and p53 signatures, which drive the execution of apoptosis, were not enriched (Figures 5A and 5B). Thus, we hypothesized that the introduction of a DNA damage signal (inherent to tumors) to *Gfi1*^{-/-} thymocytes may elicit the same increased apoptotic phenotype in thymocytes that was found in tumors. Indeed, gene expression analysis revealed that a comparison between γ -irradiated (to induce DNA damage) *Gfi1*^{-/-} versus *Gfi1*^{+/+} thymocytes recapitulated the exaggerated *Gfi1*^{-/-} GSEA DNA damage and p53 signatures found in leukemia cells (compare Figures 4B and 5B). Moreover, DNA damage induced by daunorubicin, etoposide, or by various doses of γ irradiation resulted in significantly decreased *Gfi1*^{-/-} thymocyte survival and mitochondrial potential (Figures S4A–S4E). Although *Gfi1*^{-/-} thymocytes showed similar levels of γ H2AX, p53 induction, and p53 phosphorylation compared to *Gfi1*^{+/+} controls (Figures S4F and S4G), *Gfi1*^{-/-} thymocytes displayed increased cleaved caspase-3 and PARP (Figures S4H and S4I). These data indicate that *Gfi1* antagonizes DNA damage-induced apoptotic pathways downstream of DNA damage detection but upstream of caspase and PARP1 cleavage.

To analyze this in more detail, the expression of cell death-associated p53 targets such as *Bax*, *Pmaip1* (Noxa), and *Bbc3* (*Puma*) was tested and found to be further induced in irradiated *Gfi1*^{-/-} thymocytes compared to *Gfi1*^{+/+} controls (Figure 5C).

These genes appear to be direct *Gfi1* targets because interrogation of *Gfi1* ChIP-seq data showed enriched *Gfi1* binding in the regulatory regions of *Bax*, *Pmaip1*, and *Bbc3* compared to IgG controls (Figure 5D). These data suggest that *Gfi1* co-occupies p53-responsive genes and regulates their expression. Interestingly, significant p53 binding to these same *Gfi1*-bound regions within the promoters (underscored in Figure 5D) of *Bax*, *Pmaip1*, and *Bbc3* was observed in thymocytes after induction of p53 by irradiation (Figure 5E). To assess whether *Gfi1* and p53 globally regulate the expression of proapoptotic p53 effector genes, we examined the leading edge of the GSEA *Gfi1*^{-/-}-irradiated thymocyte signature and found that >70% of the apoptotic genes were in fact proapoptotic effectors (Figure S4J). Moreover, combining the gene expression and ChIP-seq analyses revealed that *Gfi1* occupies 55 of 77 p53-effector genes (>70%) deregulated in irradiated *Gfi1*^{-/-} thymocytes (Figure 5F). We next validated the ChIP-seq data with ChIP-qPCR using primer sets for 14 of the 55 genes. These genes were (1) occupied by *Gfi1* according to ChIP-seq data with reads over 100 compared to Ig controls, (2) at least 1.5-fold differentially expressed between *Gfi1*^{-/-} and *Gfi1*^{+/+} thymocytes after irradiation, and (3) known p53 effector genes according to empirically tested data in the Molecular Signature Database (MSigDB). ChIP-qPCR confirmed binding of *Gfi1* in irradiated thymocytes with an enrichment of >1.5-fold in 10 of the 14 genes tested, suggested *Gfi1* binding in 3 genes with an enrichment of 1.3–1.5, and demonstrated little to no binding in only 1 of the 14 primer sets tested (Figure S4K). Co-occupation of the same loci by *Gfi1* and p53 was found in the majority of genes tested (9 of 14, Figure S4L). A time-dependent analysis on 4 of the 14 loci (*Bax*, *Pmaip1*, *Bbc3*, and *Cdkn1a*) revealed that a co-occupation by *Gfi1* and p53 is maintained over time but that p53 occupation clearly dominates at 120 min after the initial DNA damage signal over *Gfi1* (Figure S4M). This suggests that during the immediate response after DNA damage, *Gfi1* and p53 coregulate target genes, but if the DNA damage signal persists, a p53-dominated regulation prevails.

We investigated the involvement of the p53-activated apoptosis pathway in *Gfi1*^{-/-} thymocyte survival after DNA damage. To do so, we deleted *Trp53* or overexpressed *Bcl2* and found that either condition completely rescued the exaggerated *Gfi1*^{-/-} thymocyte apoptosis upon DNA damage signaling (Figure 5G). Further investigation into the underlying

(C) Change of thymic surface area before and after treatment with plpC for mice (see B).

(D) Top view shows *Notch1*^{ΔCT}; *Gfi1*^{fl/fl} or *Notch1*^{ΔCT}; *Mx1-Cre*⁺; *Gfi1*^{fl/fl} mice that were treated with ENU and subsequently monitored by ultrasound for tumor (T) development. Upon appearance of a mass, mice were injected with plpC and followed for tumor progression or regression by ultrasound. Bottom view is a Kaplan-Meier curve. Inset presents a PCR analysis of allele excision (Δ).

(E) Representative ultrasound images of tumors before and after plpC injection. Scale bars, 20 mm.

(F) Change of thymic surface area before and after treatment with plpC (see E).

(G) Top view shows *Gfi1*^{fl/fl} tumors or tumors that had one *Gfi1* allele deleted (*Mx1-Cre*⁺; *Gfi1*^{fl/Δ}) were transplanted into CD45.1 recipient mice, which were then treated with plpC. Bottom view is a Kaplan-Meier curve.

(H) T-ALL cell lines 5151, 5046, and 5010 were transduced with retrovirus vectors expressing *Gfi1*^{N382S} and dsRed or dsRed alone. dsRed was measured over time by FACS and normalized to the level at 48 hr. One of three representative experiments is shown.

(I) Top view shows *Gfi1*^{fl/fl} or *Mx1-Cre*⁺; *Gfi1*^{fl/fl} mice that were injected with ENU. Fifty days later, they were treated with plpC. Twenty-eight days later, they were irradiated, and transplanted with wild-type CD45.1 BM cells, then followed for survival. Bottom view is a Kaplan-Meier curve. One *Gfi1*^{fl/fl} mouse was sacrificed for morbidity unrelated to leukemia.

(J) BM of mice in (I) at the end of observation was examined for contribution of the CD45.2 (host BM) and CD45.1 (donor BM).

Vertical line (|) in all Kaplan-Meier curves indicates censored mice. Mean and mean ± SEM are shown unless stated otherwise. *p < 0.05, **p < 0.01.

See also Figure S2.

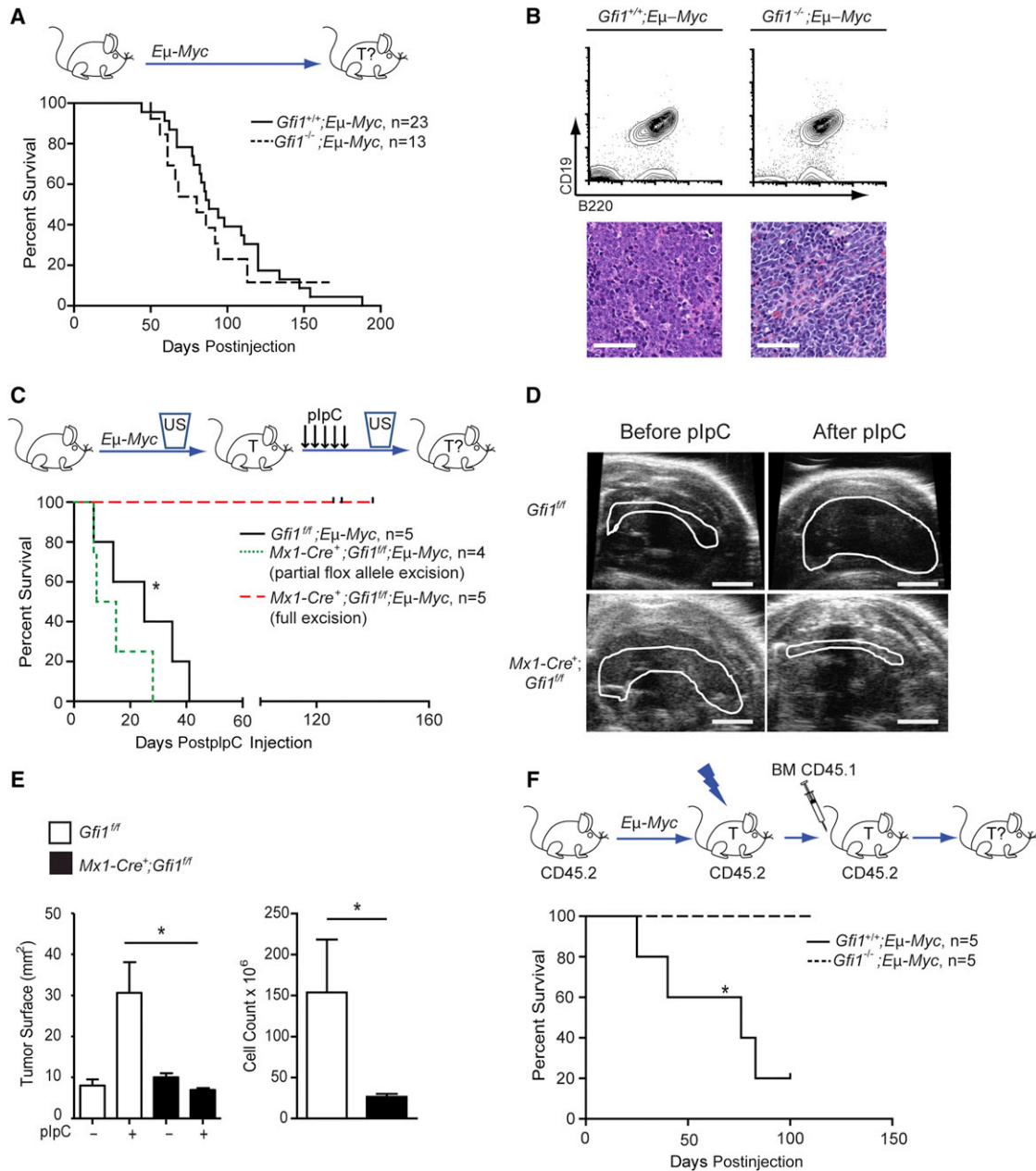


Figure 3. Gfi1 Is Required for Maintenance of B Cell Lymphoma

(A) Top view shows *Gfi1*^{+/+};*Eμ-Myc* and *Gfi1*^{-/-};*Eμ-Myc* mice that were monitored for tumor development and survival. Bottom view is a Kaplan-Meier curve.

(B) Flow cytometric analysis (top) and histological sections (bottom) of *Eμ-Myc*-induced *Gfi1*^{+/+} and *Gfi1*^{-/-} tumors. Scale bars, 50 μm.

(C) Top view shows *Mx1-Cre*⁺;*Gfi1*^{fl/fl};*Eμ-Myc* and *Gfi1*^{fl/fl};*Eμ-Myc* mice that were observed by ultrasound for appearance of B cell lymphoma. Upon appearance of a mass, mice were injected with plpC and monitored for tumor progression and survival. Bottom view is a Kaplan-Meier curve.

(D) Representative ultrasound images of tumors before and after plpC injection. Scale bars, 20 mm.

(E) Change of tumor surface area (left) before and after treatment with plpC for mice with the indicated genotypes as well as cellularity of mediastinal tumor after treatment (right).

(F) Top view shows *Gfi1*^{+/+};*Eμ-Myc* and *Gfi1*^{-/-};*Eμ-Myc* animals that were observed until enlarged lymph nodes evidenced tumor development, then they were irradiated and transplanted with CD45.1 BM cells and monitored for survival. Bottom view is a Kaplan-Meier curve.

Vertical line (|) in all Kaplan-Meier curves indicates censored mice. Mean and mean ± SEM are shown unless stated otherwise. *p < 0.05.

See also Figure S3.

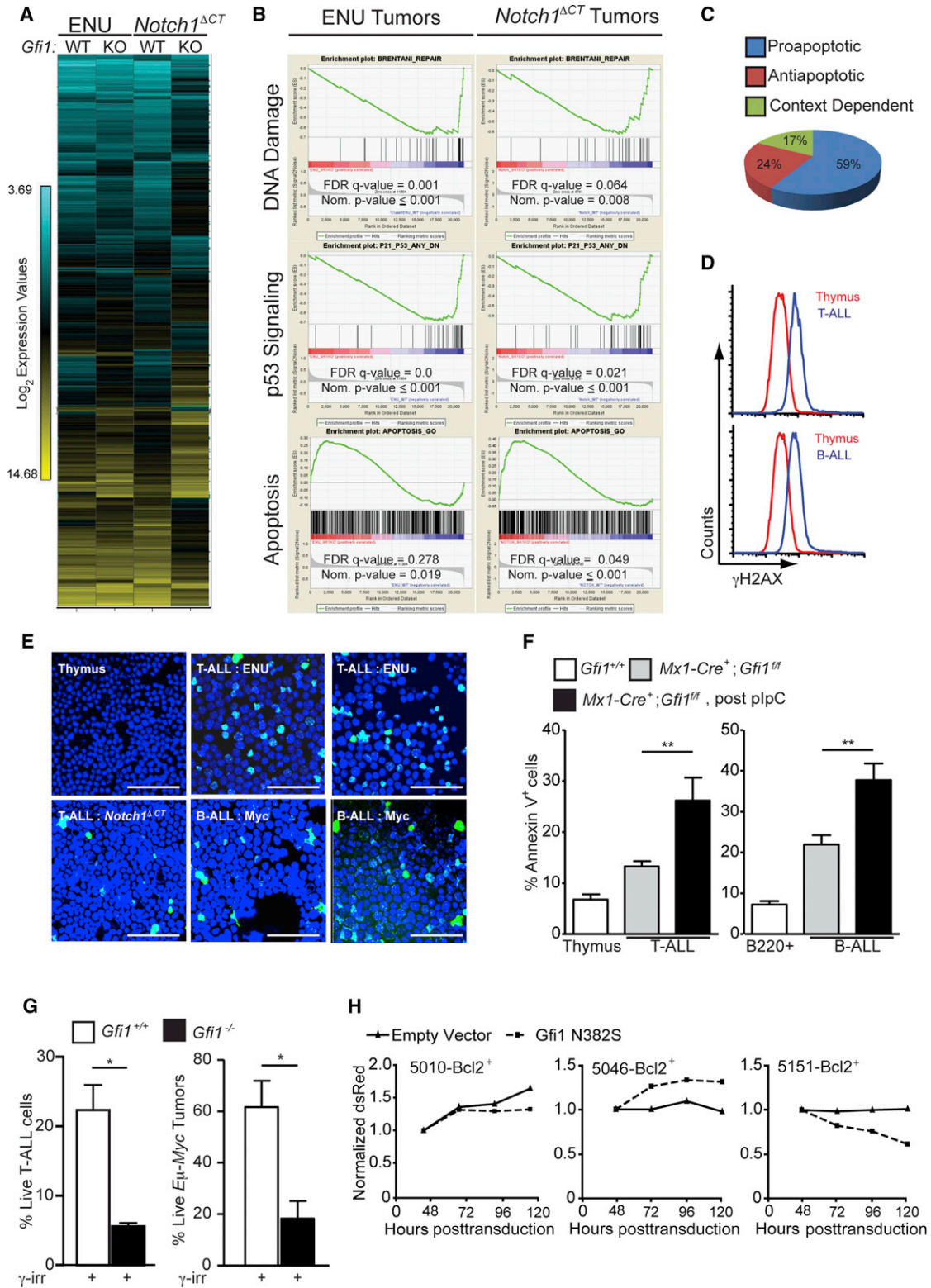


Figure 4. Gfi1 Mediates DNA Damage and p53 Signaling to Control Apoptosis

(A) Unsupervised hierarchical clustering of the averaged normalized Log₂ gene expression values from ENU (n = 3) or ENU/*Notch1^{ΔCT}* (n = 2)-induced T-ALL arising in *Gfi1^{fl/fl}* (wild-type, WT) or *Mx1-Cre⁺; Gfi1^{fl/fl}* (knockout, KO) plpC-treated mice (ENU WT, n = 3; ENU KO, n = 3; ENU/*Notch1^{ΔCT}* WT, n = 2; ENU/*Notch1^{ΔCT}* KO, n = 2).

(B) GSEA butterfly plots for pathways related to DNA damage, p53 signaling, or apoptosis found in both ENU- and *Notch1^{ΔCT}*-initiated tumor signatures from (A).

(legend continued on next page)

mechanism demonstrated that Gfi1 and p53 can physically interact in transfected cells and in irradiated thymocytes (Figures 5H and 5I) and that Gfi1 was able to repress p53-mediated transcriptional activation of a model reporter gene (Figure 5J). Notably, methylation of p53 at K372 leads to increased stability of chromatin-bound p53 and to the activation of p53 target genes, whereas demethylation of K372 has an inhibitory effect on p53 (West and Gozani, 2011). Immunoprecipitation and immunoblot experiments with *Gfi1*^{+/+} and *Gfi1*^{-/-} thymocytes showed that absence of Gfi1 leads to a substantial increase of p53-K372me, regardless of irradiation (Figure 5K). Moreover, thymocytes from knockin mice expressing only a Gfi1^{P2A} mutant (Fiolka et al., 2006) that lacks the ability to bind LSD1 (Saleque et al., 2007) also displayed a substantial increase of p53-K372me (Figure 5L). These data suggest that Gfi1 restricts p53 activity through Gfi1 SNAG-dependent cofactor recruitment and p53 demethylation (Figure 5M).

Targeting GFI1 in Human ALL Leads to Tumor Death

To test whether Gfi1 could be a suitable target for therapy of human leukemia, we used human T-ALL cell lines and reduced Gfi1 expression either by transduction of previously described shRNA-expressing lentiviral vectors (Velu et al., 2009) or Vivo-Morpholinos (Morcos et al., 2008) specifically designed against *GFI1*. In both cases, reduction of Gfi1 impeded the growth of T-ALL cell lines, which correlated with a higher level of apoptosis (Figures 6A–6C and S5A–S5C), suggesting that T-ALL is sensitive to the induction of apoptosis. When we used the pan-Bcl2 inhibitors Obatoclox and ABT-263 on three independent T-ALL lines, we observed IC₅₀ values approximately 10-fold lower than those observed in acute myeloid leukemia (AML), where the use of these drugs is currently in clinical trials (Figure 6D). Inhibition of Gfi1 further increased the efficiency of both Obatoclox treatment (Figure 6E) and radiation therapy (Figure S5D). To demonstrate the contribution of p53 to Gfi1 loss-of-function apoptosis, we used Vivo-Morpholinos to first antagonize p53 expression then Gfi1 expression. We observed a significant decrease in the ability of the Gfi1 Vivo-Morpholinos to induce apoptosis after p53 Vivo-Morpholino pretreatment (Figure S5E). Similar results were obtained using p53-targeting shRNA lentiviruses followed by Gfi1 Vivo-Morpholino treatment (data not shown).

Next, we examined Gfi1 inhibition in primary patient samples. Due to the significant limitations of in vitro systems to support primary T-ALL cell survival, we transplanted primary patient specimens into immune-deficient Nod/Scid/IL2R γ ^{-/-}

(NSG) mice then tested whether targeting Gfi1 using morpholinos is a viable approach to treat leukemia. The cells were allowed to engraft and expand for 4 days before the mice were injected with Vivo-Morpholinos over a 3 week period and monitored for survival. Gfi1 Vivo-Morpholino-treated animals showed a trend toward increased survival after only three injections (Figures S5F–S5I). We repeated the assay with samples from a patient who failed to respond to current therapies but increased the treatment frequency. When control morpholino (NT)-treated mice became moribund, we analyzed the tissues of all of the transplanted mice for the presence of human T-ALL cells. Targeting Gfi1 significantly impeded the expansion of the human leukemia in the BM, peripheral blood, and the spleen of the transplanted NSG mice (Figures 6F–6H), whereas treatment of healthy mice with the same dosing regimen did not lead to adverse effects (Figure S5J).

DISCUSSION

Important roles for Gfi1 in normal lymphoid development and acceleration of murine T cell leukemia have previously been established (Blyth et al., 2001; Chakraborty et al., 2008; Dabrowska et al., 2009; Gilks et al., 1993; Scheijen et al., 1997; Schmidt et al., 1996; Uren et al., 2008; Yücel et al., 2003). Yet, questions remained whether Gfi1 was required for the development or maintenance of human lymphoid leukemia. In the current study, we found that ablation of Gfi1 leads to regression of already established murine lymphoid neoplasms occurring through the induction of p53-dependent apoptotic pathways. Our results indicate that leukemic cells in general require Gfi1 because the ablation of Gfi1 led to lymphoid tumor regression and host survival independently of the transforming pathway or tumor etiology. It is thus conceivable that Gfi1 is an “oncerequisite” factor, a normal cellular protein upon which malignant cells uniquely depend for their survival. This offers a different paradigm for cancer therapeutics and suggests that normal cellular proteins, independent of their mutation status in human tumors, can be excellent targets for clinical intervention.

Our findings are surprising given the recently identified function of Gfi1 in myeloproliferative disease (MPD) and AML, where Gfi1 loss of function derepresses HoxA9, Meis1, and Pbx1, and can cooperate with other oncogenic lesions to transform myeloid progenitors (Horman et al., 2009). Furthermore, a SNP in the human *GFI1* deregulates *HOXA9* expression and increases the risk for human AML by 60% (Khandanpour et al.,

(C) Classification of genes in the leading edge of the GSEA apoptosis signature in (B) as Proapoptotic, Antiapoptotic, or Context Dependent.

(D and E) Determination of γ H2AX levels in normal tissue as well as in B and T cell leukemia by FACS (D) and immunofluorescence (E). One experiment was performed. Scale bars, 50 μ m.

(F) Level of spontaneous apoptosis in the indicated tissues and tumors before and after *Gfi1* deletion. T-ALL: *Gfi1*^{+/+}, n = 4; *Gfi1*^{fff}, n = 17; *Gfi1* ^{Δ/Δ} , n = 5. B-ALL: *Gfi1*^{+/+}, n = 4; *Gfi1*^{fff}, n = 13; *Gfi1* ^{Δ/Δ} , n = 4.

(G) *Gfi1*^{+/+} (n = 7), *Gfi1*^{-/-} and *Gfi1* ^{Δ/Δ} (one constitutive Gfi1 KO tumor and two tumors, in which Gfi1 has been deleted with more than 50% excision, n = 3), thymic tumor cells and *Gfi1*^{+/+}; *E μ -Myc*⁺ (n = 7), and *Gfi1*^{-/-}; *E μ -Myc*⁺ (n = 3) lymphomas were explanted and irradiated (6 Gy), and examined for Annexin V staining by FACS.

(H) T-ALL cell lines 5151, 5046, and 5010 were transduced with retrovirus vectors MSCV-Bcl-2, expanded, and then transduced with vectors encoding Gfi1^{N382S} and dsRed or dsRed alone. dsRed was measured over time by FACS and normalized to the level at 48 hr. One of three representative experiments is shown. Mean and mean \pm SEM are shown unless stated otherwise. *p < 0.05, **p < 0.01.

See also Table S2.

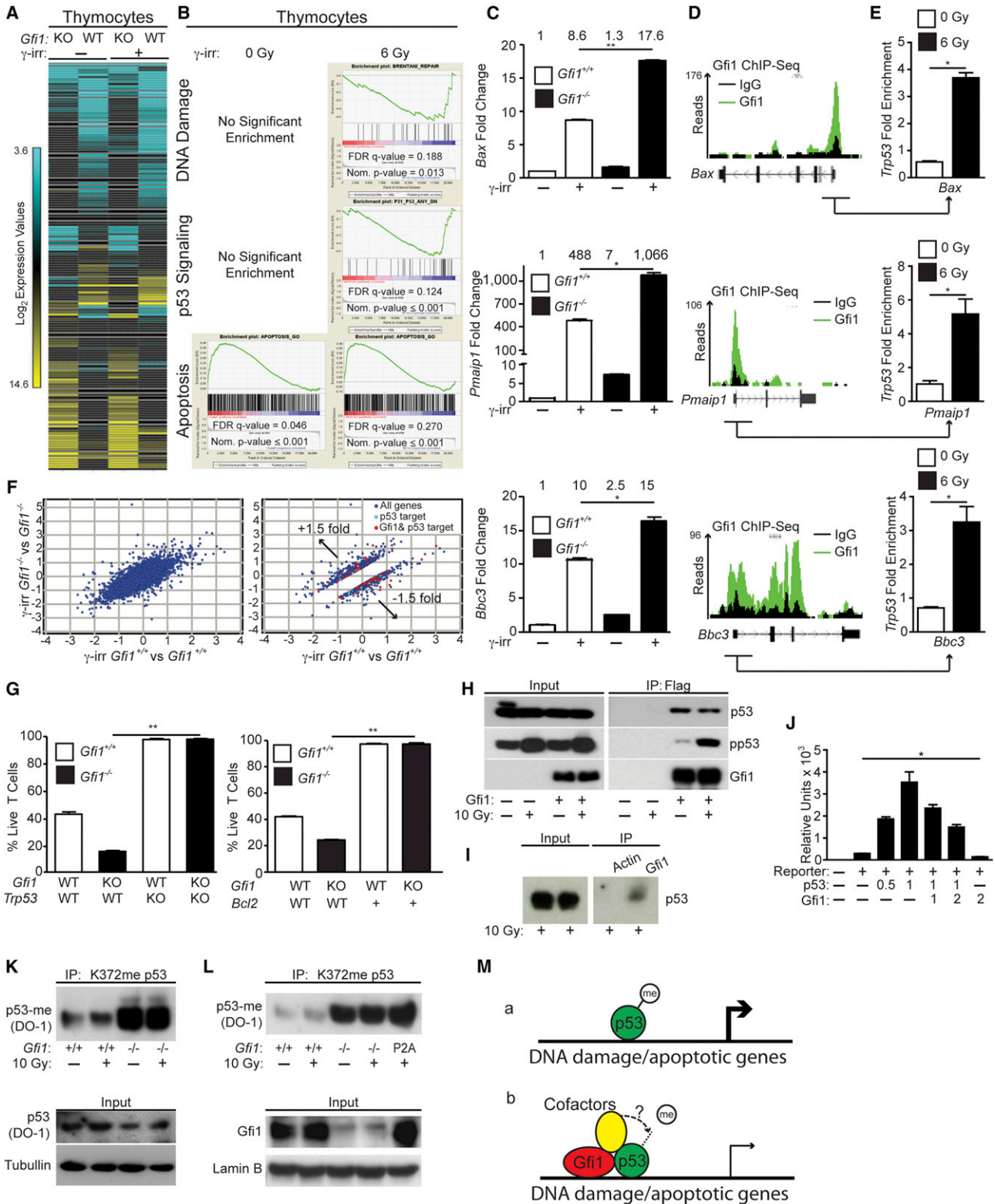


Figure 5. Gfi1 Restricts p53-Dependent Induction of Apoptosis

(A) Unsupervised hierarchical clustering of the averaged normalized Log₂ gene expression values from *Gfi1*^{+/+} (WT) and *Gfi1*^{-/-} (KO) thymocytes with or without irradiation (*Gfi1*^{+/+} control, n = 2; *Gfi1*^{-/-} control, n = 2; *Gfi1*^{+/+} irradiated, n = 3; *Gfi1*^{-/-} irradiated, n = 3).

(B) GSEA butterfly plots for pathways related to DNA damage, p53 signaling, or apoptosis enriched in Gfi1-deficient tumors (Figure 4B) that emerge in *Gfi1*^{-/-} T cells only after irradiation.

(legend continued on next page)

2012); however, further experimentation is still necessary to incisively define a role for Gfi1 in human AML. HoxA9 signaling is present in mixed-lineage leukemia but is active in less than 10% of patients with T-ALL (Ferrando et al., 2002). Thus, patients with rare HoxA9-active T-ALL may not benefit from receiving Gfi1-targeting therapies. Therefore, careful molecular pathology will likely be important to stratify patients for Gfi1-targeted therapeutics.

Recent work suggested that oncogenic signaling in general causes uncoordinated cell division resulting in collapsed replication forks and the initiation of p53-dependent DNA damage responses causing cell death (Halazonetis et al., 2008; Bartek et al., 2007; Bartkova et al., 2007; Di Micco et al., 2006). Tumor cells have to counteract this "oncogenic stress" signal to avoid cell death, for instance by mutating *TP53*. However, *TP53* mutations are rare in T-ALL; hence, leukemic cells have to devise other measures to circumvent apoptosis. Our data offer an explanation as to how lymphoid malignancies can overcome p53 activation and why they are dependent on Gfi1. We propose that DNA damage, initiated by oncogenic stress during malignant transformation, induces p53 activity. High Gfi1-expressing subclones can thus be selected during transformation to enable global restriction of p53-mediated apoptosis. Gfi1 exerts this function by (1) co-occupying p53 target genes such as *Bax*, *Pmaip1*, and *Bbc3*; (2) binding to p53-bound transcriptional complexes; and (3) limiting the methylation of p53 at K372 thereby restricting the activity of p53 and the activation of p53 target genes.

The function of Gfi1 to limit p53-K372 methylation (p53-K369 in murine cells) (Kurash et al., 2008) appears to be dependent on its ability to bind SNAG-dependent cofactors such as LSD1. It is known that demethylation of p53 at K370 is mediated by LSD1 and prevents p53 association with coactivators such as p53BP1 (Huang et al., 2007). We propose that leukemic cells use a Gfi1-LSD1 or a Gfi1-SNAG-dependent cofactor complex to demethylate p53 at K372, which prevents

a full activation of p53 and its proapoptotic target genes. However, we cannot exclude the possibility that loss of Gfi1-SNAG-dependent transcriptional repression leads to the activation of factors, which may directly affect p53 activation/methylation status. In either case, ablation of Gfi1 leads to an accumulation of more active methylated p53, to a more efficient transactivation of proapoptotic p53 target genes, and as a consequence, to accelerated cell death. Several independent lines of evidence support this notion including reporter gene assays, ChIP-seq data, biochemical analyses, and expression data and offer a mechanistic explanation why Gfi1 ablation leads to regression of murine lymphomas and causes an inhibition of primary human T-ALL cell expansion in immunodeficient mice.

Our findings have direct implications for current ALL treatments, which consist of chemotherapy and irradiation. Both are nonspecific and highly toxic, damaging host and tumor tissues. These therapies function mainly through the induction of DNA damage and the initiation of p53-dependent DNA damage response pathways that cause cell death. Even when effective, patients can suffer dramatic side effects from standard ALL treatments. Therefore, reducing chemotherapeutic or irradiation dose and thus their side effects while maintaining their efficacy would directly benefit patients. The main result from our study suggests that this goal can be achieved by inhibiting the function of Gfi1 in patients with T-ALL because ablation of Gfi1 accelerates p53-induced cell death in leukemic cells. According to our data, leukemic cells lacking Gfi1 will be more sensitive to DNA damage-inducing chemo- or irradiation therapy and undergo accelerated apoptosis. It is thus conceivable that targeting Gfi1 will not only significantly improve response rates but may in particular allow lower effective doses of chemotherapeutic agents or irradiation. In summary, our findings suggest that Gfi1 represents an Achilles' heel of lymphoid leukemias, and our approach to target Gfi1 may soon move to clinical trials.

(C) Expression of *Bax*, *Pmaip1* (*Noxa*), and *Bbc3* (*Puma*) in *Gfi1*^{+/+} and *Gfi1*^{-/-} thymocytes before and after irradiation. One representative experiment out of at least two experiments is shown. The numbers above the bars represent the mean values of the measurements.

(D) Peaks across the *Bax*, *Pmaip1*, and *Bbc3* loci from Gfi1 ChIP-seq of murine hematopoietic progenitor cells immortalized by retroviral transduction of an MLL-ENL expression vector (GSE31657).

(E) ChIP of p53 using primers from Gfi1-bound regions (underscored with arrow in D) of *Bax*, *Pmaip1*, and *Bbc3* before and after irradiation. Represented are the mean and SD of the fold difference compared to IgG control from one experiment with three technical repeats.

(F) Log₂ values of the fold change of the irradiated versus unirradiated gene expression values of all genes (left) or 1.5-fold differentially regulated (right) between *Gfi1*^{+/+} and *Gfi1*^{-/-} thymocytes. Gfi1-bound (identified in D) p53 target genes are shown in red.

(G) Percentage of live *Gfi1*^{+/+}; *Trp53*^{+/+}, *Gfi1*^{-/-}; *Trp53*^{+/+}, *Gfi1*^{+/+}; *Trp53*^{-/-}, and *Gfi1*^{-/-}; *Trp53*^{-/-} thymocytes after ex vivo γ irradiation (left, n = 3). Percentage of live *Gfi1*^{+/+}, *Gfi1*^{-/-}, *Gfi1*^{+/+}; *Vav-Bcl2*, and *Gfi1*^{-/-}; *Vav-Bcl2* thymocytes after ex vivo γ irradiation (right, n = 3).

(H) Immunoblot of total-cell lysate (left) and immunoprecipitation (right) were performed using p53, phospho-p53, or Gfi1 antibodies on lysates from untreated or irradiated 293T cells transfected as indicated with FLAG-tagged Gfi1 constructs. One representative experiment from at least two experiments is shown.

(I) Immunoblot of total-cell lysate (left) and immunoprecipitation using either Gfi1 or an isotype control (actin) antibody (right) were performed using phospho-p53 (Ser15) antibody on lysates from irradiated thymocytes cells. One representative experiment from at least two experiments is shown.

(J) Reporter expression assay using the *Bax* promoter and various amounts (μ g) of transfected vectors encoding p53 or Gfi1.

(K) Thymocytes from the indicated mice were irradiated or left untreated. After 30 min, total-cell lysates were immunoprecipitated with an anti-mono-methyl K372 p53 antibody, then immunoblotted with an anti-p53 antibody. p53 and tubulin in total-cell lysates are also shown. One experiment out of at least two experiments is shown.

(L) Thymocyte nuclear extracts from the indicated mouse strains were immunoprecipitated with an anti-mono-methyl K372 p53 antibody, then immunoblotted with an anti-p53 antibody. Input control shows the level of Gfi1 in thymocytes from *Gfi1*^{+/+}, *Gfi1*^{-/-}, and *Gfi1*^{P2A/P2A} mice and the loading control LaminB. One experiment out of at least two experiments is shown.

(M) Schematic representation showing methylated p53 binds to DNA and robustly activates the expression of target genes (a), and Gfi1 co-occupancy of a subset of p53 targets tethers a Gfi1 SNAG-dependent cofactor, which demethylates p53 to dampen the expression of p53 target gene (b).

Mean and \pm mean SEM are shown unless stated otherwise. *p < 0.05, **p < 0.01.

See also Figure S4.

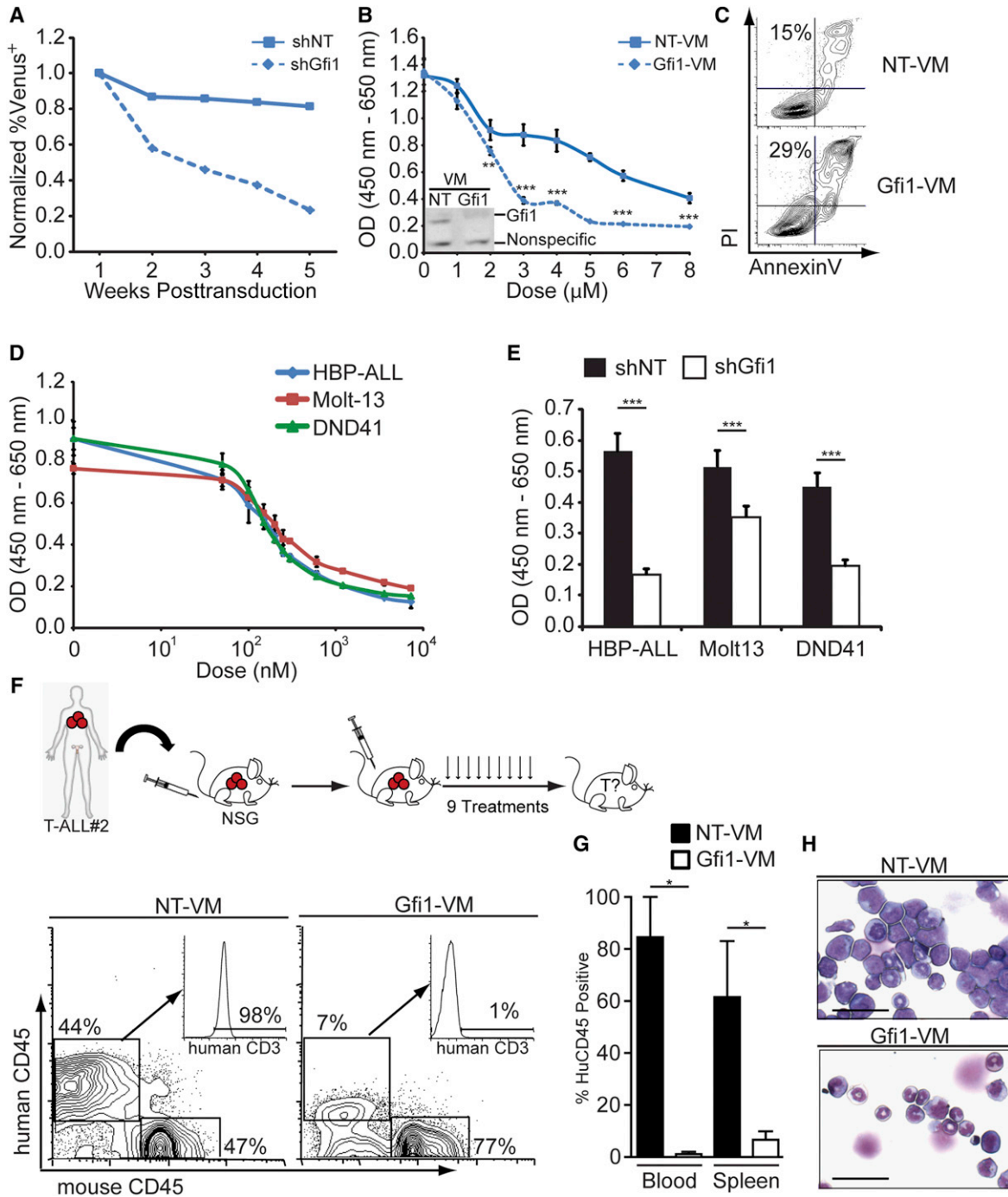


Figure 6. Gfi1 as a Target to Treat Human Leukemia

(A) HBP-ALL cells were transduced with Venus-marked shRNA-expressing lentiviral vectors targeting Gfi1 (shGfi1, dotted line) or nontargeting control (shNT, solid line). Expression of Venus was measured by FACS 72 hr posttransduction, which was set as 1, and subsequent measurements were taken by FACS over a 5 week period and normalized to the first reading, $p = 0.058$.

(B) Growth of HBP-ALL cells treated with Gfi1 or NT Vivo-Morpholinos (VM) as measured by WST assay for 48 hr. Inset shows immunoblot for Gfi1 in HBP-ALL cells treated with NT or Gfi1-VM (4 μ M) for 16 hr.

(C) Annexin V and PI staining of HBP-ALL cells after 16 hr of Gfi1 or NT VM treatment (4 μ M).

(D) Growth of T-ALL cell lines treated with indicated doses of the Obatoclax as measured by WST assay for 48 hr.

(E) Gfi1 knockdown was combined with Obatoclax treatment (200 nM), and growth was measured by WST assay for 48 hr. One representative experiment is shown; experiments were repeated two to three times (A–E).

(F) Top view shows primary patient T-ALL samples that were transplanted in NSG mice and then mice were injected with Gfi1 or NT VM three times per week for 3 weeks. Bottom view is a FACS analysis of human CD45 and human CD3 of NT ($n = 2$) or Gfi1-treated ($n = 3$) mice.

(legend continued on next page)

EXPERIMENTAL PROCEDURES

All other experimental procedures can be found in the [Supplemental Information](#).

Mice

LckCre⁺, *Mx1-Cre⁺*, C57BL/6, CD45.1, *Trp53^{-/-}*, and NSG mice were obtained from The Jackson Laboratory (Bar Harbor, ME, USA). Regarding other mouse strains, please refer to the [Supplemental Experimental Procedures](#). Mice were housed in either single ventilated cages with top filters or microisolator cages. The Institutional Animal Care, Use and Ethical Committees responsible for Cincinnati Children's Hospital Medical Center (CCHMC), the Institut de Recherches Cliniques de Montréal (IRCM), and University Clinic Essen (UKE) reviewed and approved all animal experimentation.

Xenograft Transplants and Morpholino Treatment

Diagnostic patient samples were obtained after informed consent according to Helsinki declaration and with approval from the institutional review boards at the IRCM, CCHMC, and UKE for the described experiments. One million T-ALL cells were transplanted (i.v.) into NSG mice that were injected 4 days later (i.v.) with Vivo-Morpholinos (Gene Tools) as described in [Figures 6 and S5](#) with 25 nM of control ("NT-VM," 5'-CCTCTTACCTCAGTTACAATT TATA-3') or Gfi1-specific ("Gfi1-VM," 5'-ATGGTGGTCCGGCACTTCCCCACT-3') Vivo-Morpholinos per injection.

In Vivo Deletion of Gfi1 and Ultrasound Observation

Gfi1^{fl/fl} or *RosaCre^{ERT2} Gfi1^{fl/fl}* mice were injected (i.p.) with 1 mg OHT (Sigma-Aldrich) dissolved in 100 μ l of corn oil the first 5 days following transplantation. *Gfi1^{fl/fl}* or *Mx1-Cre⁺;Gfi1^{fl/fl}* mice were either injected (i.p.) 4 weeks after the last ENU injection or 3 days after the transplantation of the tumor cells with 500 mg plpC (Sigma-Aldrich) seven times every other day. PCR validation of in vivo deletion was performed as previously described ([Horman et al., 2009](#)). Ultrasound observation was performed on anesthetized mice, and thymic tumors were measured using the Visualsonic ultrasound machine and the Vev0770 imaging software (Toronto). A tumor was called present if the thymic surface area measured in the horizontal and sagittal plane was larger than 8 mm² because average thymic surface of age-matched, untreated *Gfi1^{fl/fl}* control mice is 4 mm², and if the tumor exhibited growth of more than 50% during the last 2 weeks of observation.

Statistics

GraphPad Prism software (GraphPad Software, La Jolla, CA, USA) was used for most statistical analysis. Kaplan-Meier curves were analyzed using log rank tests. A p value ≤ 0.05 was considered significant for all analyses. Differences in incidences of leukemia or lymphoma among the different groups were determined using Fisher's exact test. Two-tailed unpaired Student's t tests were used to calculate the differences in the gene expression of patient data, WBC, and spleen weights of transplanted mice, as well as the differences in cell number or tumors in ENU and MMLV-treated mice. The Mann-Whitney U test was used to determine significance in counterselection assays. Two-way ANOVAs were used to calculate significance of Vivo-Morpholino dose-responsive curves. Differences in Annexin V staining of *Bcl2*-transgenic *Gfi1^{-/-}* mice and *Trp53p53^{-/-}Gfi1^{-/-}* were calculated using one-way ANOVAs. GSEA FDR Q values < 0.25 were used as a cutoff for enriched signatures.

ACCESSION NUMBERS

Array data are accessible under GEO accession number GSE32910.

SUPPLEMENTAL INFORMATION

Supplemental Information includes five figures, two tables, and Supplemental Experimental Procedures and can be found with this article online at <http://dx.doi.org/10.1016/j.ccr.2013.01.011>.

ACKNOWLEDGMENTS

We thank David Hildeman, Anil Jegga, Patrick Zweidler-McKay, Michelle Kelliher, Tom Look, and Paul Jolicouer for expertise and for kindly providing plasmids, cell lines, reagents, and mice. C.K. was supported by a fellowship of the Cole Foundation, the IFZ fellowship of the University Clinic of Essen, and a Max-Eder fellowship from the German Cancer fund. J.D.P. is a Pelotonia Fellow and was supported by the University of Cincinnati Cancer Therapeutics T32 training grant (T32-CA117846). J.S. was supported by a Gordon Piller PhD studentship from Leukaemia and Lymphoma Research UK, S.R.H. by a fellowship from CancerFree Kids, and J.Z. and W.E.P. by the Division of Intramural Research, National Institute of Allergy and Infectious Diseases. H.L.G. was supported by the Leukemia and Lymphoma Society of America, NIH CA105152, CA159845, Alex's Lemonade Stand, and thanks the Center of Excellence in Molecular Hematology P30 award (DK090971). T.M. was supported by a Canada Research Chair (Tier 1) and grants from the Canadian Institutes of Health Research (CIHR, MOP-84238, MOP-111011). C.K. and J.D.P. designed and performed experiments, analyzed data, and wrote the manuscript. M.-C.G., L.V., J.S., R.C., S.R.H., J.K., and B.G. performed experiments and assisted analyses. J.Z. and W.E.P. provided the *Gfi1^{fl/fl}* mouse strain. U.D. provided funding and oversaw research. H.L.G. and T.M. were responsible for concept and design of experiments, oversaw research, wrote the manuscript, and provided funding.

Received: December 22, 2011

Revised: September 11, 2012

Accepted: January 18, 2013

Published: February 11, 2013

REFERENCES

- Adams, J.M., Harris, A.W., Pinkert, C.A., Corcoran, L.M., Alexander, W.S., Cory, S., Palmeter, R.D., and Brinster, R.L. (1985). The c-myc oncogene driven by immunoglobulin enhancers induces lymphoid malignancy in transgenic mice. *Nature* 318, 533–538.
- Bartek, J., Bartkova, J., and Lukas, J. (2007). DNA damage signalling guards against activated oncogenes and tumour progression. *Oncogene* 26, 7773–7779.
- Bartkova, J., Horejsí, Z., Sehested, M., Nesland, J.M., Rajpert-De Meyts, E., Skakkebaek, N.E., Stucki, M., Jackson, S., Lukas, J., and Bartek, J. (2007). DNA damage response mediators MDC1 and 53BP1: constitutive activation and aberrant loss in breast and lung cancer, but not in testicular germ cell tumours. *Oncogene* 26, 7414–7422.
- Blyth, K., Terry, A., Mackay, N., Vaillant, F., Bell, M., Cameron, E.R., Neil, J.C., and Stewart, M. (2001). Runx2: a novel oncogenic effector revealed by in vivo complementation and retroviral tagging. *Oncogene* 20, 295–302.
- Chakraborty, J., Okonta, H., Bagalb, H., Lee, S.J., Fink, B., Changanamkandath, R., and Duggan, J. (2008). Retroviral gene insertion in breast milk mediated lymphomagenesis. *Virology* 377, 100–109.
- Coustan-Smith, E., Mullighan, C.G., Onciu, M., Behm, F.G., Raimondi, S.C., Pei, D., Cheng, C., Su, X., Rubnitz, J.E., Basso, G., et al. (2009). Early T-cell precursor leukaemia: a subtype of very high-risk acute lymphoblastic leukaemia. *Lancet Oncol.* 10, 147–156.

(G) Quantification of total human CD45⁺ cells in the blood and spleen from mice in (F).

(H) Cytospins of the BM from mice in (F). Scale bars, 50 μ m.

Mean and mean \pm SEM are shown unless stated otherwise. *p < 0.05, **p < 0.01, ***p < 0.001.

See also [Figure S5](#).

- Cullion, K., Draheim, K.M., Hermance, N., Tammam, J., Sharma, V.M., Ware, C., Nikov, G., Krishnamoorthy, V., Majumder, P.K., and Kelliher, M.A. (2009). Targeting the Notch1 and mTOR pathways in a mouse T-ALL model. *Blood* 113, 6172–6181.
- Dabrowska, M.J., Dybkaer, K., Johnsen, H.E., Wang, B., Wabl, M., and Pedersen, F.S. (2009). Loss of microRNA targets in the 3' untranslated region as a mechanism of retroviral insertional activation of growth factor independence 1. *J. Virol.* 83, 8051–8061.
- Di Micco, R., Fumagalli, M., Cicalese, A., Piccinin, S., Gasparini, P., Luise, C., Schurra, C., Garre', M., Nuciforo, P.G., Bensimon, A., et al. (2006). Oncogene-induced senescence is a DNA damage response triggered by DNA hyper-replication. *Nature* 444, 638–642.
- Ferrando, A.A., Neuberg, D.S., Staunton, J., Loh, M.L., Huard, C., Raimondi, S.C., Behm, F.G., Pui, C.H., Downing, J.R., Gilliland, D.G., et al. (2002). Gene expression signatures define novel oncogenic pathways in T cell acute lymphoblastic leukemia. *Cancer Cell* 1, 75–87.
- Fiolka, K., Hertzano, R., Vassen, L., Zeng, H., Hermesh, O., Avraham, K.B., Dührsen, U., and Möry, T. (2006). Gfi1 and Gfi1b act equivalently in haematopoiesis, but have distinct, non-overlapping functions in inner ear development. *EMBO Rep.* 7, 326–333.
- Gilks, C.B., Bear, S.E., Grimes, H.L., and Tschlis, P.N. (1993). Progression of interleukin-2 (IL-2)-dependent rat T cell lymphoma lines to IL-2-independent growth following activation of a gene (Gfi-1) encoding a novel zinc finger protein. *Mol. Cell. Biol.* 13, 1759–1768.
- Gökbuget, N., and Hoelzer, D. (2009). Treatment of adult acute lymphoblastic leukemia. *Semin. Hematol.* 46, 64–75.
- Halazonetis, T.D., Gorgoulis, V.G., and Bartek, J. (2008). An oncogene-induced DNA damage model for cancer development. *Science* 319, 1352–1355.
- Hameyer, D., Loonstra, A., Eshkind, L., Schmitt, S., Antunes, C., Groen, A., Bindels, E., Jonkers, J., Krimpenfort, P., Meuwissen, R., et al. (2007). Toxicity of ligand-dependent Cre recombinases and generation of a conditional Cre deleter mouse allowing mosaic recombination in peripheral tissues. *Physiol. Genomics* 31, 32–41.
- Horman, S.R., Velu, C.S., Chaubey, A., Bourdeau, T., Zhu, J., Paul, W.E., Gebelein, B., and Grimes, H.L. (2009). Gfi1 integrates progenitor versus granulocytic transcriptional programming. *Blood* 113, 5466–5475.
- Huang, J., Sengupta, R., Espejo, A.B., Lee, M.G., Dorsey, J.A., Richter, M., Opravil, S., Shiekhhattar, R., Bedford, M.T., Jenuwein, T., and Berger, S.L. (2007). p53 is regulated by the lysine demethylase LSD1. *Nature* 449, 105–108.
- Khandanpour, C., Krongold, J., Schütte, J., Bouwman, F., Vassen, L., Gaudreau, M.C., Chen, R., Calero-Nieto, F.J., Diamanti, E., Hannah, R., et al. (2012). The human GFI136N variant induces epigenetic changes at the Hoxa9 locus and accelerates K-RAS driven myeloproliferative disorder in mice. *Blood* 120, 4006–4017.
- Kundu, M., Compton, S., Garrett-Beal, L., Stacy, T., Starost, M.F., Eckhaus, M., Speck, N.A., and Liu, P.P. (2005). Runx1 deficiency predisposes mice to T-lymphoblastic lymphoma. *Blood* 106, 3621–3624.
- Kurash, J.K., Lei, H., Shen, Q., Marston, W.L., Granda, B.W., Fan, H., Wall, D., Li, E., and Gaudet, F. (2008). Methylation of p53 by Set7/9 mediates p53 acetylation and activity in vivo. *Mol. Cell* 29, 392–400.
- Li, H., Ji, M., Klarmann, K.D., and Keller, J.R. (2010). Repression of Id2 expression by Gfi-1 is required for B-cell and myeloid development. *Blood* 116, 1060–1069.
- Margolin, A.A., Palomero, T., Sumazin, P., Califano, A., Ferrando, A.A., and Stolovitzky, G. (2009). ChIP-on-chip significance analysis reveals large-scale binding and regulation by human transcription factor oncogenes. *Proc. Natl. Acad. Sci. USA* 106, 244–249.
- Medyouf, H., Gusscott, S., Wang, H., Tseng, J.C., Wai, C., Nemirovsky, O., Trumpp, A., Pflumio, F., Carboni, J., Gottardis, M., et al. (2011). High-level IGF1R expression is required for leukemia-initiating cell activity in T-ALL and is supported by Notch signaling. *J. Exp. Med.* 208, 1809–1822.
- Morcós, P.A., Li, Y., and Jiang, S. (2008). Vivo-Morpholinos: a non-peptide transporter delivers Morpholinos into a wide array of mouse tissues. *Biotechniques* 45, 613–614, 616, 618 passim.
- Murtaugh, L.C., Stanger, B.Z., Kwan, K.M., and Melton, D.A. (2003). Notch signaling controls multiple steps of pancreatic differentiation. *Proc. Natl. Acad. Sci. USA* 100, 14920–14925.
- O'Neil, J., Grim, J., Strack, P., Rao, S., Tibbitts, D., Winter, C., Hardwick, J., Welcker, M., Meijerink, J.P., Pieters, R., et al. (2007). FBW7 mutations in leukemic cells mediate NOTCH pathway activation and resistance to gamma-secretase inhibitors. *J. Exp. Med.* 204, 1813–1824.
- Palomero, T., Lim, W.K., Odom, D.T., Sulis, M.L., Real, P.J., Margolin, A., Barnes, K.C., O'Neil, J., Neuberg, D., Weng, A.P., et al. (2006). NOTCH1 directly regulates c-MYC and activates a feed-forward-loop transcriptional network promoting leukemic cell growth. *Proc. Natl. Acad. Sci. USA* 103, 18261–18266.
- Pargmann, D., Yücel, R., Kosan, C., Saba, I., Klein-Hitpass, L., Schimmer, S., Heyd, F., Dittmer, U., and Möry, T. (2007). Differential impact of the transcriptional repressor Gfi1 on mature CD4+ and CD8+ T lymphocyte function. *Eur. J. Immunol.* 37, 3551–3563.
- Person, R.E., Li, F.Q., Duan, Z., Benson, K.F., Wechsler, J., Papadaki, H.A., Eliopoulos, G., Kaufman, C., Bertolone, S.J., Nakamoto, B., et al. (2003). Mutations in proto-oncogene GFI1 cause human neutropenia and target ELA2. *Nat. Genet.* 34, 308–312.
- Priceputu, E., Bouallaga, I., Zhang, Y., Li, X., Chrobak, P., Hanna, Z.S., Poudrier, J., Kay, D.G., and Jolicoeur, P. (2006). Structurally distinct ligand-binding or ligand-independent Notch1 mutants are leukemogenic but affect thymocyte development, apoptosis, and metastasis differently. *J. Immunol.* 177, 2153–2166.
- Saleque, S., Kim, J., Rooke, H.M., and Orkin, S.H. (2007). Epigenetic regulation of hematopoietic differentiation by Gfi-1 and Gfi-1b is mediated by the cofactors CoREST and LSD1. *Mol. Cell* 27, 562–572.
- Scheijen, B., Jonkers, J., Acton, D., and Berns, A. (1997). Characterization of pal-1, a common proviral insertion site in murine leukemia virus-induced lymphomas of c-myc and Pim-1 transgenic mice. *J. Virol.* 71, 9–16.
- Schmidt, T., Zörnig, M., Beneke, R., and Möry, T. (1996). MoMuLV proviral integrations identified by Sup-F selection in tumors from infected myc/pim bitransgenic mice correlate with activation of the gfi-1 gene. *Nucleic Acids Res.* 24, 2528–2534.
- Schmidt, T., Karsunky, H., Gau, E., Zevnik, B., Elsässer, H.P., and Möry, T. (1998). Zinc finger protein GFI-1 has low oncogenic potential but cooperates strongly with pim and myc genes in T-cell lymphomagenesis. *Oncogene* 17, 2661–2667.
- Sharma, V.M., Calvo, J.A., Draheim, K.M., Cunningham, L.A., Hermance, N., Beverly, L., Krishnamoorthy, V., Bhasin, M., Capobianco, A.J., and Kelliher, M.A. (2006). Notch1 contributes to mouse T-cell leukemia by directly inducing the expression of c-myc. *Mol. Cell. Biol.* 26, 8022–8031.
- Spooner, C.J., Cheng, J.X., Pujadas, E., Laslo, P., and Singh, H. (2009). A recurrent network involving the transcription factors PU.1 and Gfi1 orchestrates innate and adaptive immune cell fates. *Immunity* 31, 576–586.
- Subramanian, A., Tamayo, P., Mootha, V.K., Mukherjee, S., Ebert, B.L., Gillette, M.A., Paulovich, A., Pomeroy, S.L., Golub, T.R., Lander, E.S., and Mesirov, J.P. (2005). Gene set enrichment analysis: a knowledge-based approach for interpreting genome-wide expression profiles. *Proc. Natl. Acad. Sci. USA* 102, 15545–15550.
- Thompson, B.J., Buonamici, S., Sulis, M.L., Palomero, T., Vilimas, T., Basso, G., Ferrando, A., and Aifantis, I. (2007). The SCFFBW7 ubiquitin ligase complex as a tumor suppressor in T cell leukemia. *J. Exp. Med.* 204, 1825–1835.
- Uren, A.G., Kool, J., Matentzoglou, K., de Ridder, J., Mattison, J., van Uiter, M., Lagcher, W., Sie, D., Tanger, E., Cox, T., et al. (2008). Large-scale mutagenesis in p19(ARF)- and p53-deficient mice identifies cancer genes and their collaborative networks. *Cell* 133, 727–741.
- Van Vlierberghe, P., van Grotel, M., Tchinda, J., Lee, C., Beverloo, H.B., van der Spek, P.J., Stubbs, A., Cools, J., Nagata, K., Fornerod, M., et al. (2008).

- The recurrent SET-NUP214 fusion as a new HOXA activation mechanism in pediatric T-cell acute lymphoblastic leukemia. *Blood* 111, 4668–4680.
- Velu, C.S., Baktula, A.M., and Grimes, H.L. (2009). Gfi1 regulates miR-21 and miR-196b to control myelopoiesis. *Blood* 113, 4720–4728.
- Weng, A.P., Ferrando, A.A., Lee, W., Morris, J.P., 4th, Silverman, L.B., Sanchez-Irizarry, C., Blacklow, S.C., Look, A.T., and Aster, J.C. (2004). Activating mutations of NOTCH1 in human T cell acute lymphoblastic leukemia. *Science* 306, 269–271.
- Weng, A.P., Millholland, J.M., Yashiro-Ohtani, Y., Arcangeli, M.L., Lau, A., Wai, C., Del Bianco, C., Rodriguez, C.G., Sai, H., Tobias, J., et al. (2006). c-Myc is an important direct target of Notch1 in T-cell acute lymphoblastic leukemia/lymphoma. *Genes Dev.* 20, 2096–2109.
- West, L.E., and Gozani, O. (2011). Regulation of p53 function by lysine methylation. *Epigenomics* 3, 361–369.
- Yuan, Y., Zhou, L., Miyamoto, T., Iwasaki, H., Harakawa, N., Hetherington, C.J., Burel, S.A., Lagasse, E., Weissman, I.L., Akashi, K., and Zhang, D.E. (2001). AML1-ETO expression is directly involved in the development of acute myeloid leukemia in the presence of additional mutations. *Proc. Natl. Acad. Sci. USA* 98, 10398–10403.
- Yücel, R., Karsunky, H., Klein-Hitpass, L., and Möröy, T. (2003). The transcriptional repressor Gfi1 affects development of early, uncommitted c-Kit+ T cell progenitors and CD4/CD8 lineage decision in the thymus. *J. Exp. Med.* 197, 831–844.
- Zarebski, A., Velu, C.S., Baktula, A.M., Bourdeau, T., Horman, S.R., Basu, S., Bertolone, S.J., Horwitz, M., Hildeman, D.A., Trent, J.O., and Grimes, H.L. (2008). Mutations in growth factor independent-1 associated with human neutropenia block murine granulopoiesis through colony stimulating factor-1. *Immunity* 28, 370–380.
- Zhu, J., Jankovic, D., Grinberg, A., Guo, L., and Paul, W.E. (2006). Gfi-1 plays an important role in IL-2-mediated Th2 cell expansion. *Proc. Natl. Acad. Sci. USA* 103, 18214–18219.
- Zörnig, M., Schmidt, T., Karsunky, H., Grzeschiczek, A., and Möröy, T. (1996). Zinc finger protein GFI-1 cooperates with myc and pim-1 in T-cell lymphomagenesis by reducing the requirements for IL-2. *Oncogene* 12, 1789–1801.

Supplemental Information

Growth Factor Independence 1 Antagonizes a p53-Induced DNA Damage Response Pathway in Lymphoblastic Leukemia

Cyrus Khandanpour, James D. Phelan, Lothar Vassen, Judith Schütte, Riyan Chen, Shane R. Horman, Marie-Claude Gaudreau, Joseph Krongold, Jinfang Zhu, William E. Paul, Ulrich Dührsen, Bertie Göttgens, H. Leighton Grimes, and Tarik Möröy

Inventory of Supplemental Information

Supplemental Data

Figure S1. Related to Figure 1.

Table S1. Related to Figure 1.

Figure S2. Related to Figure 2.

Figure S3. Related to Figure 3.

Table S2. Related to Figure 4.

Figure S4. Related to Figure 5.

Figure S5. Related to Figure 6.

Supplemental Experimental Procedures

Supplemental Reference

Supplemental Data

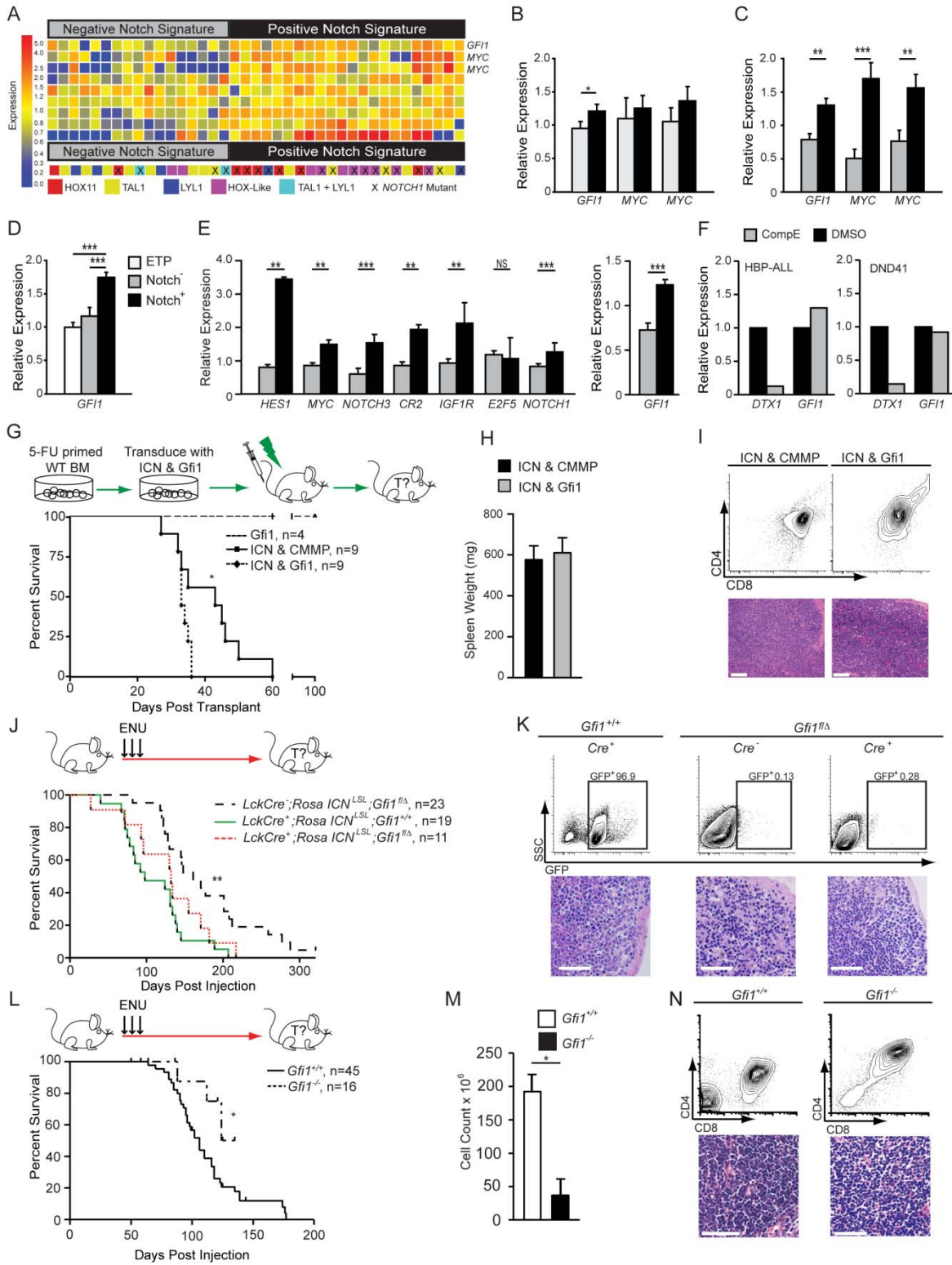


Figure S1, related to Figure 1. *Gfi1* expression is associated with a subgroup of human T-ALL and modulates T-ALL initiation

(A) Expression of published Notch1 target genes was used to classify gene expression array data from 39 T-ALL patients into two groups: “Negative Notch Signature” (grey, left) and “Positive Notch Signature” (black, right).

(B, C) Quantification of mRNA for *GFII* and two unique probes for the known ICN target gene *MYC* after clustering the patients by *NOTCH1* mutational status (B) or by ICN target gene activation (C).

(D) Expression of published Notch1 target genes or clinical diagnosis was used to classify gene expression array data from 55 T-ALL patients (GSE8879, Figure 1A) into three groups: “ETP-ALL” (white), “Negative Notch Signature” (grey) and “Positive Notch Signature” (black) and relative *GFII* expression is shown.

(E) Expression of published NOTCH1 target genes was used to classify gene expression array data from another set of 91 T-ALL patients (GSE10609) into two groups “Negative Notch Signature” (grey) and “Positive Notch Signature” (black). (Left) Quantification of mRNA for Notch1 target genes; (right) quantification of mRNA for *GFII*.

(F) Human T-ALL cell lines were cultured in complete RPMI media with 1 μ M Compound E or vehicle control (DMSO) for 16 hours. RNA was isolated and gene expression was analyzed using TaqMan probes for *GFII* (Hs00382207_m1), *DTX1* (Hs00269995_m1), and normalized to *GAPDH* (Hs00266705_g1) using the $\Delta\Delta$ CT method. One experiment was performed.

(G) Top: Scheme of experimental strategy: 5-FU treated wild-type bone marrow cells were transduced with retroviral vectors expressing GFP and ICN, or GFP alone, then with vectors

expressing DsRed and Gfi1, or DsRed alone, then transplanted into recipient mice. Bottom: Kaplan-Meier curve. ICN and Gfi1 versus ICN versus Gfi1 alone.

(H, I) Post-mortem spleen weight (H) and flow cytometric analysis of thymic tumors (I, top panels) as well as histological sections of splenic tumors (I, bottom panels).

(J) Top: *Lck-Cre⁺;RosaICN^{LSL}* (n=19), *RosaICN^{LSL};Gfi1^{f/Δ}* (n=23), and *Lck-Cre⁺;RosaICN^{LSL};Gfi1^{f/Δ}* (n=11) mice were injected with ENU. Cre-mediated deletion of a floxed stop cassette (LSL) activates ICN-IRES-eGFP. Bottom: Kaplan-Meier curve.

(K) Flow cytometric analysis (top panels) and histological sections (bottom panels) from tumors arising in *RosaICN^{LSL};Gfi1^{f/Δ}*, *Lck-Cre⁺RosaICN^{LSL}*, and *Lck-Cre⁺RosaICN^{LSL}Gfi1^{f/Δ}* mice.

(L) Top: ENU injected *Gfi1^{+/+}* (n=45) and *Gfi1^{-/-}* (n=16) mice were monitored for tumor development and survival. Bottom: Kaplan-Meier curve.

(M, N) Thymic tumor cell numbers (M) and flow cytometric analysis (N, top panels) and histological sections (N, bottom panels) of ENU induced *Gfi1^{+/+}* and *Gfi1^{-/-}* tumors. Scale in histological sections represents 50μm.

| in all Kaplan-Meier curve plots indicate censored mice.

Mean and ±SEM are shown unless stated otherwise. *p<0.05, **p<0.01, ***p<0.001.

Table S1, related to Figures 1. ENU-induced T cell malignancies from *Gfi1*^{+/+} and *Gfi1*^{-/-} mice do not harbor mutations in *Notch1* domains associated with T-ALL.

Mouse ENU-treatment	<i>Notch1</i> Domain (bp sequenced):		
	HD-TAD (4775-6419)	HD-PEST (6321-7708)	PEST-Stop (7241-7881)
<i>Gfi1</i> ^{+/+} R1	-	-	-
<i>Gfi1</i> ^{+/+} R2	-	-	-
<i>Gfi1</i> ^{+/+} R3	-	-	-
<i>Gfi1</i> ^{+/+} R4	-	-	-
<i>Gfi1</i> ^{-/-} R1	-	-	-
<i>Gfi1</i> ^{-/-} R2	-	-	-
<i>Gfi1</i> ^{-/-} R3	-	-	-

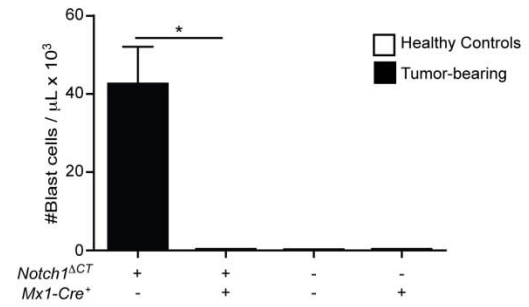
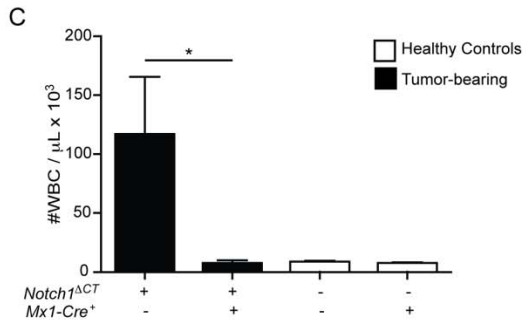
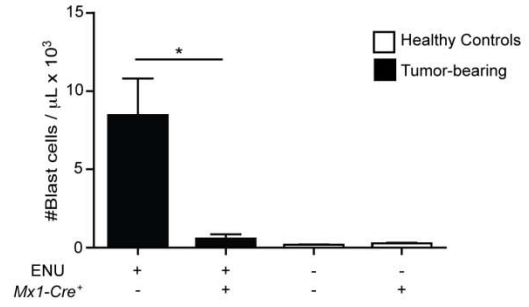
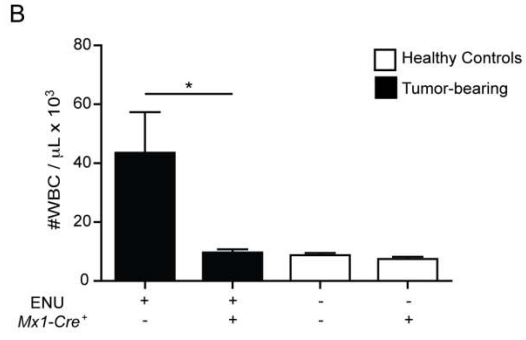
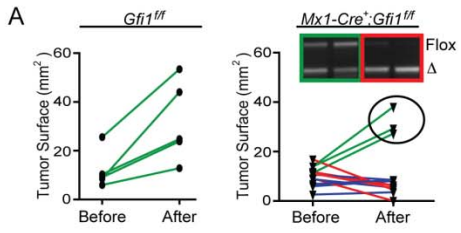


Figure S2, related to Figure 2. *Gfi1* is critical for T-ALL tumor maintenance

(A) Tumor surface area (arising from mice described in Figure 2B) was examined by ultrasound before and after pIpC injection in *Gfi1^{fl/fl}* (left) and *Mx1-Cre⁺;Gfi1^{fl/fl}* (right) mice. Mice in which tumor surface area increased after pIpC treatment are shown in green, those that remained unchanged are in blue, and those that decreased are displayed in red. Insert: PCR analysis of the *Gfi1* locus in representative tumors for *Gfi1* flox and excised (Δ) alleles.

(B) As described in Figure 2B, *Gfi1^{fl/fl}* (n=6) or *Mx1-Cre⁺;Gfi1^{fl/fl}* (n=4) mice were treated with ENU and subsequently monitored by ultrasound for tumor development. Upon appearance of a mass, mice were injected with pIpC and followed for tumor progression or regression by ultrasound. At the end of observation, the number of white blood cells (WBC, left) and leukemic “Blast” cells (right) in the peripheral blood was determined and compared to results of healthy pIpC injected *Mx1-Cre⁺;Gfi1^{fl/fl}* and *Gfi1^{fl/fl}* mice (n=3 for both groups).

(C) As described in Figure 2D, *Notch1 ^{Δ CT};Gfi1^{fl/fl}* (n=2) or *Notch1 ^{Δ CT};Mx1-Cre⁺;Gfi1^{fl/fl}* (n=3) mice were treated with ENU and subsequently monitored by ultrasound for tumor development. Upon appearance of a mass, mice were injected with pIpC and followed for tumor progression or regression by ultrasound. At the end of observation, the number of white blood cells (WBC, left) and leukemic “Blast” cells (right) in the peripheral blood was determined and compared to results of healthy pIpC injected *Mx1-Cre⁺;Gfi1^{fl/fl}* and *Gfi1^{fl/fl}* mice (n=3 for both groups).

| in all Kaplan-Meier curve plots indicate censored mice.

Mean and \pm SEM are shown unless stated otherwise. *p<0.05.

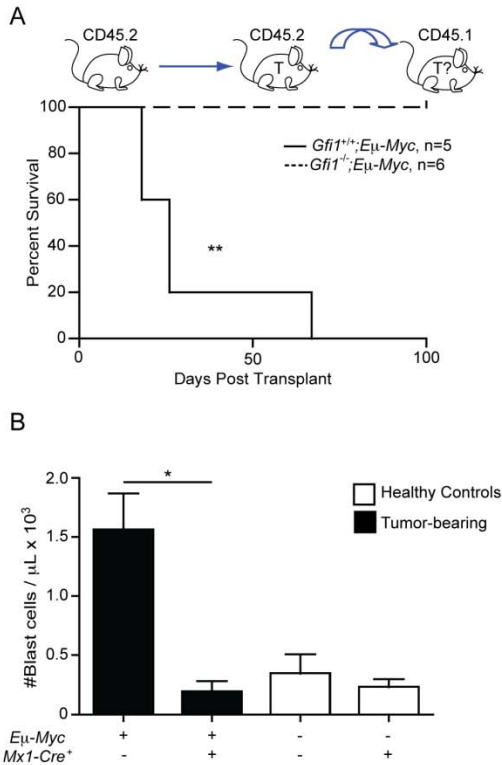


Figure S3, related to Figure 3. *Gfi1* is critical for B-ALL tumor maintenance

(A) Lymphomas from *Gfi1*^{+/+}; *Eμ-Myc* (black line) and *Gfi1*^{-/-}; *Eμ-Myc* (dotted line) mice (CD45.2, Figure 3A) were transplanted into sublethally irradiated congenic recipients (CD45.1) which were monitored for tumor progression and host survival.

(B) As described in Figure 3C, *Mx1-Cre*⁺; *Gfi1*^{fl/fl}; *Eμ-Myc* and *Gfi1*^{fl/fl}; *Eμ-Myc* mice were observed by ultrasound for appearance of B-cell lymphoma. Upon appearance of a mass, mice were injected with pIpC and monitored for tumor progression and survival. At end of observation, the number of leukemic “Blast” cells in the peripheral blood of these mice was determined and compared to results of healthy pIpC injected *Mx1-Cre*⁺; *Gfi1*^{fl/fl} and *Gfi1*^{fl/fl} mice (n=3 for each group).

Mean and \pm SEM are shown unless stated otherwise. *p<0.05, **p < 0.01.

Table S2, related to Figure 4. GSEA Signatures.

Please see Excel file.

GSEA signatures are displayed in indicated pathways from Gfi1 sufficient (*Gfi1*^{+/+} or *Gfi1*^{f/f}) or Gfi1 deficient (*Gfi1*^{-/-} or *Gfi1*^{Δ/Δ}) T cells, irradiated T cells, ENU-induced tumors, or *Notch1*^{ΔCT} ENU accelerated tumors.

Depicted GSEA signatures are shown where at least one comparison between matched tissues resulted in an FDR q-value <0.25.

GSEA signatures highlighted in blue represent signatures statistically enriched in DNA damage containing matched tissues, but not in unirradiated T cells.

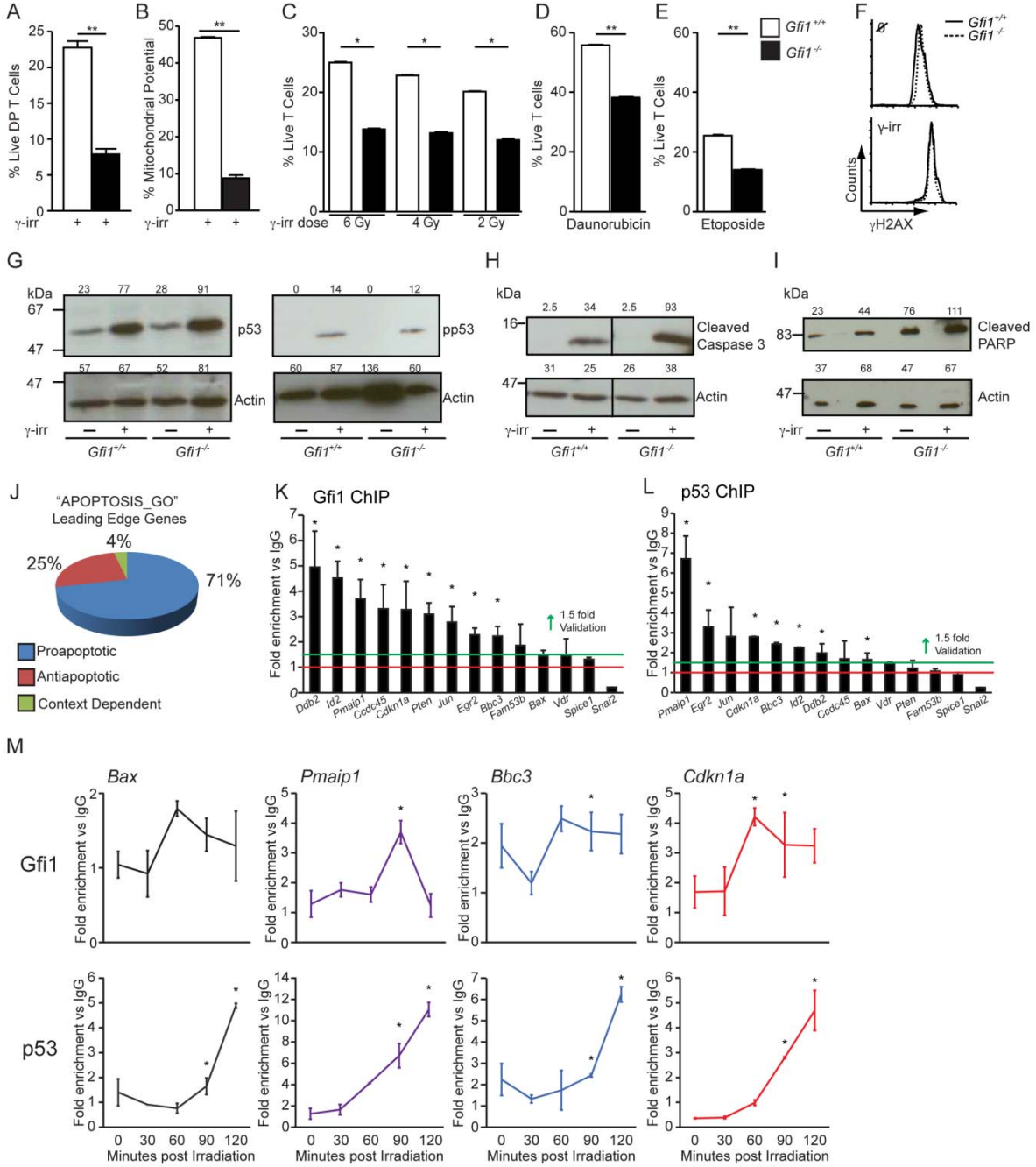


Figure S4, related to Figure 5. *Gfi1*^{-/-} thymocytes are more sensitive to apoptosis after p53-induced DNA damage.

(A) Percentage of AnnexinV negative CD4⁺CD8⁺ FACS sorted thymocytes from *Gfi1*^{+/+} and *Gfi1*^{-/-} mice after *ex vivo* γ -irradiation (n=3 for each genotype from one experiment).

(B) Thymocytes from *Gfi1*^{+/+} and *Gfi1*^{-/-} mice were explanted and γ -irradiated. Mitochondrial membrane potential was measured by JC-1 dye fluorescence in the FITC and PE channels by flow cytometry. The percent of thymocytes showing dye fluorescence in both channels is shown (n=3 for each genotype from one representative experiment). Level of mitochondrial potential loss after irradiation was normalized to untreated samples.

(C-E) Percentage of AnnexinV negative thymocytes from *Gfi1*^{+/+} and *Gfi1*^{-/-} mice after various doses of *ex vivo* γ -irradiation (C), Daunorubicin (D) or Etoposide (E) treatment (n=3 for each genotype from one experiment).

(F) Flow cytometric quantification of γ H2AX in total thymocytes from *Gfi1*^{+/+} and *Gfi1*^{-/-} mice pre- and 120 min post- γ -irradiation (6 Gy) from one experiment.

(G) Immunoblot analysis of total cell lysate using antibodies against p53 (left) or phospho-p53 (right) from *Gfi1*^{+/+} and *Gfi1*^{-/-} thymocytes pre- and 180 min post irradiation (6 Gy). Numbers indicate densitometric quantification from one experiment.

(H, I) Immunoblot analysis of total cell lysate using antibodies against cleaved Caspase-3 (H) or cleaved PARP (I) from *Gfi1*^{+/+} and *Gfi1*^{-/-} total thymocytes after *ex vivo* pre- and 180 min post γ -irradiation (6 Gy). Numbers indicate densitometric quantification from one experiment.

(J) Pie chart characterizing the Leading Edge genes from the “Apoptosis_GO” GSEA signature from irradiated thymocytes according to their GO biological function.

(K, L) Wild-type thymocytes were irradiated (5 Gy) and chromatin was generated 90 minutes later. ChIP-qPCR was performed on chromatin immunoprecipitated with antibodies against Gfi1

(K) or p53 (L). Values represent the fold enrichment of binding for p53 and Gfi1 to the indicated regulatory regions of the annotated genes compared to the IgG controls from one experiment with three different technical repeats.

(M) Wild-type thymocytes were irradiated (5 Gy) and chromatin was generated 0, 30, 60, 90 and 120 minutes later. ChIP-qPCR was performed on chromatin immunoprecipitated with antibodies against Gfi1 (top) or p53 (bottom) for four of the 14 genes analyzed in (K, L). Values represent the fold enrichment of binding for p53 and Gfi1 to the indicated regulatory regions of the annotated genes compared to the IgG controls from one experiment with three different technical repeats.

Mean and \pm SEM are shown unless stated otherwise. * $p < 0.05$, ** $p < 0.01$.

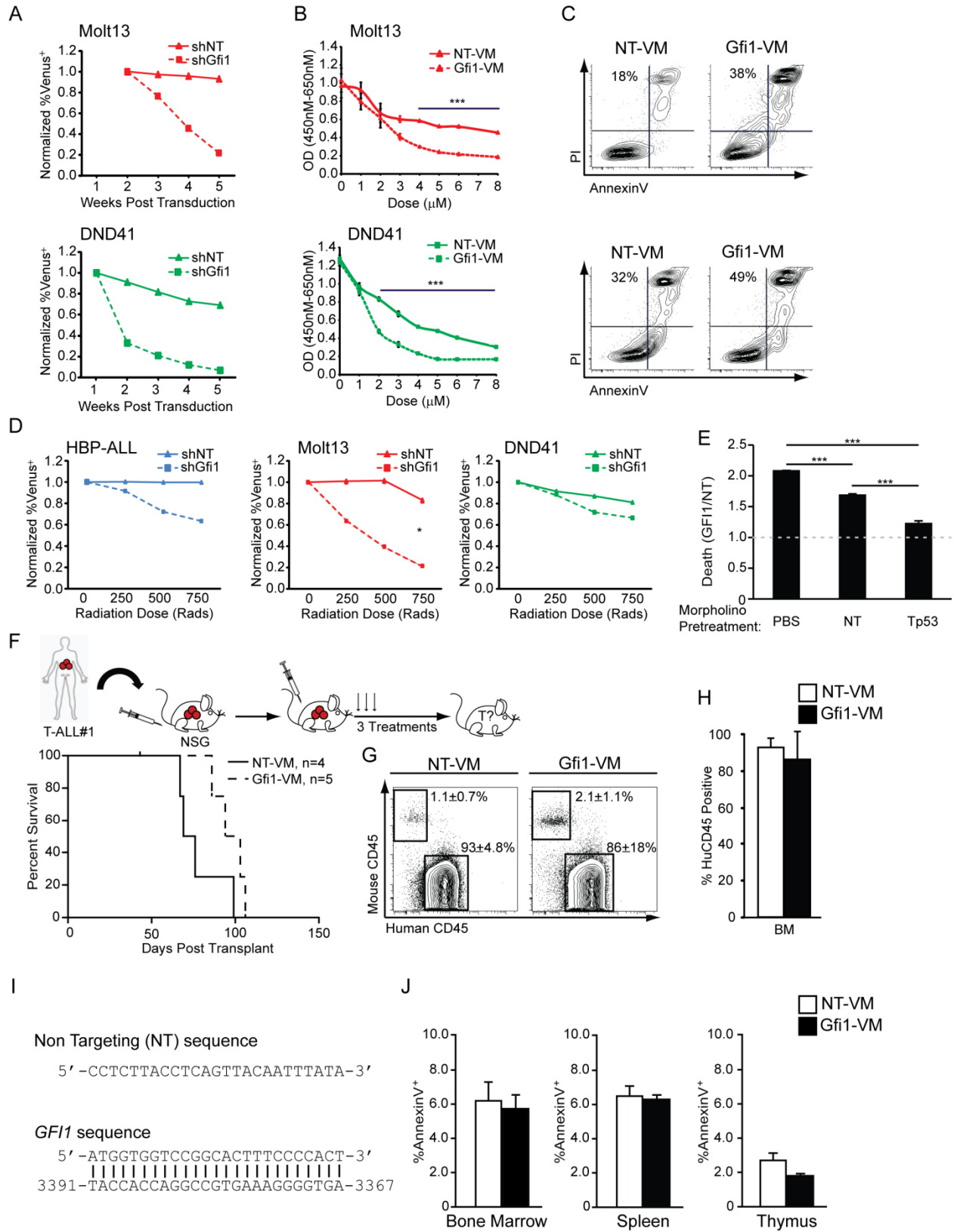


Figure S5, related to Figure 6. Loss of Gfi1 in human T-ALL induces apoptosis and tumor regression

(A) Indicated T-ALL cells were transduced with YFP marked shRNA expressing lentiviral vectors targeting Gfi1 (shGfi1, dotted line) or non-targeting control (shNT, solid line).

Expression of YFP was measured by FACS 72 hours post transduction, which was set as 1, and subsequent measurements were taken by FACS over a 5 week period and normalized to the first reading, $p=0.123$ (Molt13), $p=0.058$ (DND41).

(B) Growth of T-ALL cell lines Molt13 (top) or DND41 (bottom) treated with various doses of Gfi1 (dotted line) or NT (solid line) Vivo Morpholinos (VM) as measured by WST assay after 48 hours of VM treatment.

(C) AnnexinV and PI staining after 16 hours of culture with NT or Gfi1 VM (4 μ M) in Molt13 (top) or DND41 (bottom) cell lines. 1 of at least 3 representative experiments is shown (A-C).

(D) T-ALL cell lines were transduced with Venus-marked lentiviral shRNA control (shNT, solid line) or Gfi1 constructs (shGfi1, dotted line), plated and then irradiated at various doses. Cells were analyzed for Venus⁺ cells the following 3 days. Measurements were normalized to 1 at the first time point (non-irradiated). Graphs display data from 72 hours post irradiation. 1 of 3 different time points is shown.

(E) Molt13 cells were treated for 24 hours with PBS, NT or Tp53-specific VM (4 μ M). Media was changed and cells were replated with NT or Gfi1 VM (4 μ M). AnnexinV and PI staining was measured 24 hours later by flow cytometry. The ratio of the percent increase in dead cells with Gfi1 compared to NT VM treatment is displayed. 1 of 4 representative experiments using various T-ALL cell lines is shown.

(F) Top: Primary patient T-ALL samples passaged in NSG mice and four days later were treated (i.v.) with 12.5 mg/kg of Gfi1 or NT VM once a week for 3 weeks. Bottom: Kaplan-Meier plot of NT or Gfi1-treated VM treated mice ($p=0.07$).

(G) Post mortem FACS analysis of bone marrow for human T-ALL cells from above NSG recipient mice.

(H) Graphical representation of (G, $n=3$ for each).

(I) Sequence of the NT and Gfi1 Vivo Morpholinos.

(J) WT ($n=3$ for each group) mice were injected with either murine Gfi1-specific or NT control Vivo Morpholino once every other day for a total of 9 injections times. Two days after the last injection, indicated organs were harvested and apoptosis was measured by AnnexinV staining.

| in all Kaplan-Meier curve plots indicate censored mice.

Mean and \pm SEM are shown unless stated otherwise. * $p < 0.05$, ** $p < 0.01$, *** $p < 0.001$.

Experimental Procedures

Mouse strains

The generation of *Notch1^{ACT}*, *Gfi1^{-/-}*, *Gfi1^{ff}*, *H2^k-Bcl2-tg*, *Eμ-Myc*, *RosaCre^{ERT2}* and *RosaICN^{LSL}* mice have been previously published (Karsunky et al., 2002; Kelly et al., 2007; Kondo et al., 1997; Priceputu et al., 2006; Yang et al., 2004; Zhu et al., 2006).

Tumorigenesis assays

Transplants: Donor mice were primed with 250 mg/kg of 5-fluorouracil (5-FU) and BM cells were harvested 72 hours later. Low-density BM was fractionated by Histopaque 1083 (Sigma-Aldrich, St. Louis, MO), cytokine expanded for 48 hours, and then spin infected twice with retroviral supernatants 24 hours apart as previously reported (Horman et al., 2009). Transduction rates were determined by flow cytometry and equal numbers of transduced cells were transplanted into 6-8 week old syngenic recipients after sublethal radiation. **ENU:** Three to nine-week old mice were injected once a week (for a total length of three weeks) with 100 mg/kg of ENU. ENU-induced BM failure was defined as having a hemoglobin level lower than 8 dg/dL, platelets under 100/fL and leukocytes below 2/fL. **MMLV:** New-born mice (1-2 days old) were injected with 100 μL of MMLV (PFU 2x10⁵) as described (Schmidt et al., 1996). Secondary transplants were performed in six to ten week old CD45.1 mice after sublethal irradiation (6 Gy) and injected with 10⁵ (CD45.2) tumor cells. Engraftment was verified by the presence of 3x10⁵ CD45.2 cells, which were co-injected at the time of transplant.

In vivo deletion of Gfi1 and ultrasound observation

Gfi1^{fl/fl} or *RosaCre^{ERT2};Gfi1^{fl/fl}* mice were injected (i.p) with 1 mg OHT (Sigma-Aldrich) dissolved in 100 μ L of corn oil the first five days following transplantation. *Gfi1^{fl/fl}* or *Mx1-Cre⁺;Gfi1^{fl/fl}* mice were either injected (i.p) four weeks after the last ENU injection or three days after the transplantation of the tumor cells with 500 mg pIpC (Sigma-Aldrich) seven times every other day. PCR validation of *in vivo* deletion was performed as previously described (Horman et al., 2009). Ultra sound observation was performed on anesthetized mice and thymic tumors were measured using the Visualsonic ultrasound machine and the Vev0770 imaging software (both Toronto, Canada). A tumor was called present if the thymic surface area measured in the horizontal and sagittal plane was larger than 8 mm², as average thymic surface of age matched, untreated *Gfi1^{fl/fl}* control mice is 4 mm², and if the tumor exhibited growth of more than 50% during the last two weeks of observation.

In vitro cell culture and treatments

Thymocytes or primary tumors (purity \geq 95 % as measured by FACS) were explanted and put in culture at a concentration of 2×10^6 cells/mL/well (of a 12 well plate) in 10% fetal calf serum (FCS, Hyclone (Waltham, MA, USA), 1640 RPMI (Wilsent, Montreal, Canada)). Cells were either left untreated or irradiated (6 Gy). Six hours after irradiation, viability was measured by either using the AnnexinV staining method or by measuring loss of mitochondrial potential (JC-1 mitochondrial potential kit, Invitrogen) according to manufacturer's protocol. Values were normalized to untreated controls for both AnnexinV staining and mitochondrial membrane potential assays. For DNA damage induction by chemical, Daunorubicin was added at a concentration of (10 μ g/mL) and Etoposide at a concentration of (10 μ g/mL). Murine T-ALL

cell lines were maintained in 1640 RPMI (Gibco) with 20% FCS, 1% Pen/Strep, 1% L-glutamine and 50 mM β -mercaptoethanol. Human T-ALL cell lines were maintained in 1640 RPMI (Gibco) with 10% FBS (Gibco), 1% Pen/Strep, and 1% L-glutamine. Obatoclax (Selleck Chem.) was dissolved in DMSO and added to T-ALL cultures at indicated doses.

Sequences for Non-Targeting (SHC002,

CCGGCAACAAGATGAAGAGCACCAACTCGAGTTGGTGCTCTTCATCTTGTTGTTTTT)

and Gfi1 (TRCN0000020465,

CCGGCCAGACTATTCCCTCCGTTTACTCGAGTAAACGGAGGGAATAGTCTGGTTTTT)

shRNA were purchased in the lentiviral vector pLKO.1 (Sigma). The eYFP fluorescent marker Venus was cloned into the location of the puromycin resistance gene. Lentiviral transduction levels of T-ALL cells were determined 48-72 hours post transduction by flow cytometry.

Subsequent measurements were normalized to the initial reading. Counter-selection of *GFI1*-targeting shRNAs was observed as evidenced by >50% reduction in Venus levels over time.

γ H2AX foci

γ H2AX foci were detected by using the γ H2AX specific antibody from BD (560445).

Immunofluorescence and FACS was performed according to manufacturer's manual.

ChIP, ChIP-Seq & RT-PCR

ChIP-Seq (GSE31657) ChIP assays were performed as previously described (Forsberg et al., 2000) using a polyclonal anti-Gfi1 (abcam ab21061) antibody. Briefly, 2×10^7 MLL-ENL immortalized bone marrow progenitor cells were cross-linked in 1 % formaldehyde, lysed and sonicated in fragments of about 150 to 400 bp. Each sample was amplified using the Illumina kit

following manufacturer's instructions and sequenced using the Illumina 2G Genome Analyzer. Sequencing reads were mapped to the mouse reference genome using Bowtie converted to a density plot as described (Wilson et al., 2009), and displayed in UCSC genome browser. ChIP was performed on explanted irradiated thymocytes after treatment using similar procedures as above and an anti-p53 antibody (F1393, Santa Cruz). To detect p53 methylation, the anti-p53 (mono methyl K372) antibody (ab16033, ABCAM) was used in conjunction with the anti-p53 antibody (DO-1). This antibody also detects murine p53 methylated at K369, which corresponds to K372 in the human p53 (Kurash, JK et al., Molecular Cell, 2008). Real-Time PCR was performed with primers covering the following sites *Bax*: F-CGGCAATTCTGCTTTAACCT, R-CGCCCCATTATTTCTTCTT; *Bbc3*: F-CTTGTGCCCCAGCTTTCAT, R-GAGTCCCAGGTGCTTCCTTC; *Ccdc45*: F-CGATCTGAGAACCCGTAAGC R-GACAGCAGAGGAGCACTTCC; *Cdkn1a*: F1-CGCTGCGTGACAAGAGAATA, R1-CCTCCCCTCTGGGAATCTAA; F2- TCCTTTTCTGGGAAGTGGTG, R2-AGGTATCCTCTGGGGCTGAT; *Ddb2*: F-GAGGACCTCTGCGACTTTTG, R-CTTTTCCACTCCTTGCTTCG; *Egr2*: F-AGCGTGGGTCAAGAAAGAGA, R-GTAGCCTGGGATAGCAGACG; *Fam53b*: F-GGAAGTAGCACCGCACAAGT, R-GGTCTTGTTCCGCCACAGATT; *Id2*: F-AGGCTGACGATAGTGGGATG, R-CTCCAAGCTCAAGGAACTGG; *Jun*: F-GACACTGGGAAGCGTGTCT, R-ATGGGCACATCACCCTACA; *Pmaip1*: F-CCCAGCAATGGATACGATCT, R-GAGGACGAGTCCTGCTCAAC; *Pten*: F-ATGTGGCGGGACTCTTTGT, R-TCCGAGAGGAGAGAGCTGAG; *Snai2*: F-ATGAGCAGCCCATTTTGAAC, R-AACCAATCACAGCCAAGAGG; *Spice1*: F-CTCCACTGGGAGGTAGCAAG, R-

ACCTCCACATACCGCACTTC; *Vdr*: F-GTTAAGGACGTTGGCTGCTC, R-
AAGGTGTGTGGGACCTCTTG

Reporter assay and immunoprecipitation

Reporter and immunoprecipitation assays were performed as previously described (Khandanpour et al., 2010a; Khandanpour et al., 2010b).

Xenograft transplants and Morpholino Treatment

T-ALL #1 was immunophenotyped as a CD5⁺, CD10^(dim), surface CD3^(dim), CD4⁺, CD8⁺, CD7⁺, cytoplasmic CD3⁺, TdT⁺, CD38⁺ tumor and found to have a t(11;14) translocation by FISH. T-ALL #2 was classified as FABL2 thymic T-ALL and immunophenotyped as a CD1a⁺, CD2⁺, cytoplasmic CD3⁺, CD7⁺, CD14^(dim), CD20^(dim) tumor. NT, Gfi1 or Tp53 (5'-TAGGATCTGACTGCGGCTCCTCCAT-3') Vivo Morpholinos were added to T-ALL cell cultures at 4 μM unless otherwise stated.

Sequence generation and dosing of morpholinos:

Vivo Morpholino sequences were designed by the experts at Gene Tools, LLC (Philomath, OR) to specifically bind to the translation start site of *GFII*. Oligo sequences were next Blasted (NCBI) to verify sequence specificity and validate that other known genes were not inadvertently targeted. Downregulation of *GFII* mRNA and protein was also verified in various human T-ALL cell lines (Figure 6 and data not shown). Control non-targeting (NT) Vivo Morpholinos were also designed by the experts at Gene Tools with a sequence that does not target any known

mammalian gene sequence. All mice received approximately 60 μ L of a 500 μ M Vivo Morpholino solution (i.v.). Dosing varied between 3 to 9 injections. Blood volume of an average 0.020 kg mouse was estimated to be 1.2 mL, resulting in a 25 nM dose (per injection).

The sequence for targeting murine *Gfi1* is: TCTTGACCAGGAATGAGCGCGGCAT.

Gene expression arrays and analyses:

Gene expression arrays were performed according to published procedures (Valk et al., 2004). Microarray data was analyzed using GeneSpring (Agilent Technologies). Published microarray data for T-ALL patients was downloaded and analyzed with GeneSpring software. Data was imported into GeneSpring and the median of each probe was normalized to 1. Gene expression data was filtered for probesets of published Notch1 target genes which were in turn used for unsupervised hierarchical clustering of samples. Normalized expression values were exported, averaged by group (ie. Notch1 target gene expression, *NOTCH1* mutation status, or clinical diagnosis) and then graphed. GSEA was performed comparing each tumor or tissue type to its *Gfi1*^{-/-} counterpart against all curated gene sets in the Molecular Signature Database.

Supplemental References

Forsberg, E. C., Downs, K. M., and Bresnick, E. H. (2000). Direct interaction of NF-E2 with hypersensitive site 2 of the beta-globin locus control region in living cells. *Blood* 96, 334-339.

Karsunky, H., Zeng, H., Schmidt, T., Zevnik, B., Kluge, R., Schmid, K. W., Duhrsen, U., and Moroy, T. (2002). Inflammatory reactions and severe neutropenia in mice lacking the transcriptional repressor Gfi1. *Nat Genet* 30, 295-300.

Kelly, P. N., Dakic, A., Adams, J. M., Nutt, S. L., and Strasser, A. (2007). Tumor growth need not be driven by rare cancer stem cells. *Science* 317, 337.

Khandanpour, C., Sharif-Askari, E., Vassen, L., Gaudreau, M. C., Zhu, J., Paul, W. E., Okayama, T., Kosan, C., and Moroy, T. (2010a). Evidence that growth factor independence 1b regulates dormancy and peripheral blood mobilization of hematopoietic stem cells. *Blood* 116, 5149-5161.

Khandanpour, C., Thiede, C., Valk, P. J., Sharif-Askari, E., Nuckel, H., Lohmann, D., Horsthemke, B., Siffert, W., Neubauer, A., Grzeschik, K. H., *et al.* (2010b). A variant allele of Growth Factor Independence 1 (GFI1) is associated with acute myeloid leukemia. *Blood* 115, 2462-2472.

Kondo, M., Akashi, K., Domen, J., Sugamura, K., and Weissman, I. L. (1997). Bcl-2 rescues T lymphopoiesis, but not B or NK cell development, in common gamma chain-deficient mice. *Immunity* 7, 155-162.

Valk, P. J., Verhaak, R. G., Beijen, M. A., Erpelinck, C. A., Barjesteh van Waalwijk van Doorn-Khosrovani, S., Boer, J. M., Beverloo, H. B., Moorhouse, M. J., van der Spek, P. J., Lowenberg, B., and Delwel, R. (2004). Prognostically useful gene-expression profiles in acute myeloid leukemia. *N Engl J Med* 350, 1617-1628.

Wilson, N. K., Miranda-Saavedra, D., Kinston, S., Bonadies, N., Foster, S. D., Calero-Nieto, F., Dawson, M. A., Donaldson, I. J., Dumon, S., Frampton, J., *et al.* (2009). The transcriptional program controlled by the stem cell leukemia gene Scl/Tal1 during early embryonic hematopoietic development. *Blood* 113, 5456-5465.

Yang, X., Klein, R., Tian, X., Cheng, H. T., Kopan, R., and Shen, J. (2004). Notch activation induces apoptosis in neural progenitor cells through a p53-dependent pathway. *Dev Biol* 269, 81-94.

Table S2, related to Figure 4. GSEA Signatures.

Enriched Gene Set	Enrichment Score (ES)	False Discovery Rate (FDR) q-value
Deregulated NFkB-Signaling		
HINATA_NFKB_UP		
ENU Tumors	0.482	0.006
Irradiated T cells	0.572	0.016
Notch Tumors	0.577	0.003
T cells	0.414	0.134
REGULATION_OF_I_KAPPAB_KINASE_NF_KAPPAB_CASCADE		
ENU Tumors	0.382	0.173
Irradiated T cells	0.400	0.424
Notch Tumors	0.332	0.529
T cells	0.451	0.206
TNFA_NFKB_DEP_UP		
ENU Tumors	0.614	0.031
Irradiated T cells	0.732	0.031
Notch Tumors	0.631	0.094
T cells	0.400	0.543
Deregulated Cell cycle		
BRENTANI_CELL_CYCLE		
ENU Tumors	-0.601	0.000
Irradiated T cells	-0.441	0.238
Notch Tumors	-0.462	0.132
T cells	-0.360	0.556
CELL_CYCLE		
ENU Tumors	-0.594	0.000
Irradiated T cells	-0.501	0.123
Notch Tumors	-0.504	0.061
T cells	-0.352	0.621
CELL_CYCLE_ARREST		
ENU Tumors	-0.631	0.002
Irradiated T cells	-0.291	0.846
Notch Tumors	0.357	0.676
T cells	0.294	0.835
CELL_CYCLE_ARREST_GO_0007050		
ENU Tumors	-0.429	0.084
Irradiated T cells	-0.297	0.822
Notch Tumors	0.322	0.680
T cells	0.311	0.720
CELL_CYCLE_CHECKPOINT		
ENU Tumors	-0.658	0.003
Irradiated T cells	-0.600	0.229
Notch Tumors	-0.657	0.061
T cells	-0.634	0.211
CELL_CYCLE_CHECKPOINT_GO_0000075		
ENU Tumors	-0.666	0.000
Irradiated T cells	-0.516	0.261
Notch Tumors	-0.504	0.141
T cells	-0.384	0.789
CELL_CYCLE_GO_0007049		
ENU Tumors	-0.533	0.000
Irradiated T cells	-0.292	0.546
Notch Tumors	-0.412	0.070
T cells	-0.245	0.915

CELL_CYCLE_KEGG		
ENU Tumors	-0.545	0.001
Irradiated T cells	-0.385	0.419
Notch Tumors	-0.431	0.179
T cells	0.315	0.461
CELL_CYCLE_PHASE		
ENU Tumors	-0.620	0.000
Irradiated T cells	-0.343	0.382
Notch Tumors	-0.472	0.030
T cells	-0.331	0.756
CELL_CYCLE_PROCESS		
ENU Tumors	-0.627	0.000
Irradiated T cells	-0.335	0.380
Notch Tumors	-0.495	0.007
T cells	-0.351	0.933
CELL_CYCLE_REGULATOR		
ENU Tumors	-0.612	0.024
Irradiated T cells	-0.486	0.518
Notch Tumors	-0.342	0.819
T cells	0.352	0.725
G1_S_TRANSITION_OF_MITOTIC_CELL_CYCLE		
ENU Tumors	-0.753	0.000
Irradiated T cells	0.446	0.531
Notch Tumors	-0.386	0.662
T cells	-0.469	0.809
G1_TO_S_CELL_CYCLE_REACTOME		
ENU Tumors	-0.582	0.000
Irradiated T cells	-0.433	0.303
Notch Tumors	-0.511	0.056
T cells	-0.350	0.624
HSA04110_CELL_CYCLE		
ENU Tumors	-0.502	0.001
Irradiated T cells	-0.332	0.529
Notch Tumors	-0.445	0.094
T cells	0.273	0.599
INTERPHASE		
ENU Tumors	-0.644	0.000
Irradiated T cells	-0.331	0.626
Notch Tumors	-0.407	0.290
T cells	-0.413	0.842
INTERPHASE_OF_MITOTIC_CELL_CYCLE		
ENU Tumors	-0.640	0.000
Irradiated T cells	-0.332	0.667
Notch Tumors	-0.442	0.213
T cells	-0.409	0.801
M_PHASE		
ENU Tumors	-0.620	0.000
Irradiated T cells	-0.361	0.412
Notch Tumors	-0.518	0.017
T cells	-0.283	0.913
M_PHASE_OF_MITOTIC_CELL_CYCLE		
ENU Tumors	-0.649	0.000
Irradiated T cells	-0.449	0.210
Notch Tumors	-0.571	0.007
T cells	-0.317	0.876
MEIOTIC_CELL_CYCLE		
ENU Tumors	-0.592	0.005
Irradiated T cells	0.371	0.716
Notch Tumors	-0.466	0.321
T cells	0.386	0.539

MITOSIS		
ENU Tumors	-0.643	0.000
Irradiated T cells	-0.448	0.196
Notch Tumors	-0.570	0.006
T cells	-0.320	0.827
MITOTIC_CELL_CYCLE		
ENU Tumors	-0.637	0.000
Irradiated T cells	-0.379	0.250
Notch Tumors	-0.517	0.006
T cells	-0.312	0.768
MITOTIC_CELL_CYCLE_CHECKPOINT		
ENU Tumors	-0.753	0.000
Irradiated T cells	-0.520	0.373
Notch Tumors	-0.407	0.684
T cells	-0.324	1.000
NEGATIVE_REGULATION_OF_CELL_CYCLE		
ENU Tumors	-0.412	0.054
Irradiated T cells	-0.259	0.872
Notch Tumors	0.338	0.545
T cells	0.378	0.407
POSITIVE_REGULATION_OF_CELL_CYCLE		
ENU Tumors	-0.430	0.400
Irradiated T cells	0.392	0.771
Notch Tumors	-0.285	0.993
T cells	0.672	0.114
REGULATION_OF_CELL_CYCLE		
ENU Tumors	-0.481	0.000
Irradiated T cells	-0.298	0.612
Notch Tumors	-0.296	0.554
T cells	0.252	0.750
REGULATION_OF_MITOSIS		
ENU Tumors	-0.697	0.000
Irradiated T cells	-0.453	0.383
Notch Tumors	-0.462	0.279
T cells	-0.284	1.000
REGULATION_OF_MITOTIC_CELL_CYCLE		
ENU Tumors	-0.698	0.002
Irradiated T cells	-0.575	0.224
Notch Tumors	-0.562	0.239
T cells	0.381	0.701
Deregulated DNA damage		
BRENTANI_REPAIR		
ENU Tumors	-0.670	0.001
Irradiated T cells	-0.547	0.188
Notch Tumors	-0.625	0.064
T cells	-0.487	0.431
DNA_DAMAGE_CHECKPOINT		
ENU Tumors	-0.674	0.009
Irradiated T cells	-0.593	0.231
Notch Tumors	-0.356	0.844
T cells	-0.351	0.995
DNA_DAMAGE_RESPONSE__SIGNAL_TRANSDUCTION		
ENU Tumors	-0.492	0.073
Irradiated T cells	-0.429	0.590
Notch Tumors	-0.280	0.950
T cells	0.263	0.970
DNA_DAMAGE_SIGNALING		
ENU Tumors	-0.483	0.007
DNA_REPAIR		

ENU Tumors	-0.601	0.000
Irradiated T cells	-0.319	0.630
Notch Tumors	-0.457	0.077
T cells	-0.326	0.770
DOUBLE_STRAND_BREAK_REPAIR		
ENU Tumors	-0.611	0.013
Irradiated T cells	-0.536	0.310
Notch Tumors	-0.596	0.136
T cells	-0.401	0.863
RESPONSE_TO_DNA_DAMAGE_STIMULUS		
ENU Tumors	-0.548	0.000
Irradiated T cells	-0.354	0.378
Notch Tumors	-0.359	0.326
T cells	-0.287	0.872
Deregulated p53 Signaling		
HSA04115_P53_SIGNALING_PATHWAY		
ENU Tumors	-0.402	0.114
Irradiated T cells	0.344	0.521
Notch Tumors	0.308	0.685
T cells	0.478	0.093
KANNAN_P53_DN		
Irradiated T cells	0.591	0.196
T cells	0.648	0.089
KANNAN_P53_UP		
Notch Tumors	0.540	0.123
P21_P53_ANY_DN		
ENU Tumors	-0.688	0.000
Irradiated T cells	-0.558	0.124
Notch Tumors	-0.654	0.021
T cells	-0.483	0.399
P21_P53_MIDDLE_DN		
ENU Tumors	-0.814	0.000
Irradiated T cells	-0.614	0.187
Notch Tumors	-0.748	0.014
T cells	-0.448	0.639
P53_BRCA1_UP		
ENU Tumors	0.538	0.046
Irradiated T cells	0.290	0.840
Notch Tumors	0.563	0.078
T cells	0.276	0.869
P53_SIGNALING		
ENU Tumors	-0.346	0.192
Irradiated T cells	0.456	0.160
Notch Tumors	0.314	0.585
T cells	0.434	0.124
P53GENES_ALL		
ENU Tumors	0.390	0.548
Irradiated T cells	0.708	0.068
Notch Tumors	0.667	0.072
T cells	0.585	0.171
P53HYPOXIAPATHWAY		
Notch Tumors	0.576	0.188
Apoptosis Related Pathways		
ANTI_APOPTOSIS		
ENU Tumors	0.276	0.500
Irradiated T cells	0.414	0.380
Notch Tumors	0.415	0.236
T cells	0.469	0.126
APOPTOSIS		

ENU Tumors	0.470	0.037
Irradiated T cells	0.598	0.019
Notch Tumors	0.536	0.038
T cells	0.574	0.016
APOPTOSIS_GENMAPP		
ENU Tumors	0.371	0.312
Irradiated T cells	0.497	0.180
Notch Tumors	0.420	0.345
T cells	0.524	0.103
APOPTOSIS_GO		
ENU Tumors	0.282	0.278
Irradiated T cells	0.401	0.270
Notch Tumors	0.437	0.050
T cells	0.443	0.046
APOPTOSIS_KEGG		
ENU Tumors	0.397	0.186
Irradiated T cells	0.546	0.097
Notch Tumors	0.481	0.190
T cells	0.524	0.080
BRENTANI_DEATH		
ENU Tumors	0.318	0.405
Irradiated T cells	0.549	0.083
Notch Tumors	0.333	0.588
T cells	0.455	0.143
HSA04210_APOPTOSIS		
ENU Tumors	0.414	0.096
Irradiated T cells	0.438	0.206
Notch Tumors	0.355	0.453
T cells	0.415	0.193
INDUCTION_OF_APOPTOSIS_BY_EXTRACELLULAR_SIGNALS		
ENU Tumors	0.308	0.748
Irradiated T cells	0.441	0.544
Notch Tumors	0.573	0.129
T cells	0.555	0.219
INDUCTION_OF_APOPTOSIS_BY_INTRACELLULAR_SIGNALS		
ENU Tumors	-0.569	0.046
Irradiated T cells	-0.392	0.731
Notch Tumors	0.525	0.306
T cells	0.472	0.453
NEGATIVE_REGULATION_OF_APOPTOSIS		
ENU Tumors	0.262	0.501
Irradiated T cells	0.408	0.386
Notch Tumors	0.450	0.117
T cells	0.515	0.035
NEGATIVE_REGULATION_OF_PROGRAMMED_CELL_DEATH		
ENU Tumors	0.262	0.539
Irradiated T cells	0.408	0.385
Notch Tumors	0.450	0.119
T cells	0.515	0.035
PASSERINI_APOPTOSIS		
ENU Tumors	0.443	0.133
Irradiated T cells	0.631	0.034
Notch Tumors	0.539	0.098
T cells	0.690	0.002
PROGRAMMED_CELL_DEATH		
ENU Tumors	0.282	0.272
Irradiated T cells	0.401	0.275
Notch Tumors	0.437	0.049
T cells	0.443	0.045
REGULATION_OF_APOPTOSIS		

ENU Tumors	0.261	0.377
Irradiated T cells	0.391	0.324
Notch Tumors	0.428	0.087
T cells	0.466	0.034
REGULATION_OF_PROGRAMMED_CELL_DEATH		
ENU Tumors	0.261	0.380
Irradiated T cells	0.391	0.330
Notch Tumors	0.428	0.088
T cells	0.466	0.034